This is to certify that the

thesis entitled

THE CHEMISTRY OF FIRST ROW TRANSITION METAL IONS WITH PRIMARY AMINES IN THE GAS PHASE: CORRELATIONS OF REACTIVITY WITH ELECTRONIC STRUCTURE

presented by

Susan J. Babinec

has been accepted towards fulfillment
of the requirements for

M.S. degree in Chemistry

John Allison
Major professor

Date 5 JAN. 1987

THE CHEMISTRY OF FIRST ROW TRANSITION METAL IONS WITH PRIMARY AMINES IN THE GAS PHASE: CORRELATIONS OF REACTIVITY WITH ELECTRONIC STRUCTURE

BY

Susan J. Babinec

A DISSERTATION

Submitted to

Michigan State University

in partial fulfillment of the requirements

for the degree of

MASTER OF SCIENCE

Department of Chemistry

1984

ABSTRACT

THE CHEMISTRY OF FIRST ROW TRANSITION METAL IONS WITH PRIMARY AMINES IN THE GAS PHASE: CORRELATIONS OF REACTIVITY WITH ELECTRONIC STRUCTURE

By

Susan J. Babinec

In the past several years, an extensive body of literature has appeared in the area of gas phase organometallic ion/molecule reactions. Most of the observed reactions can be explained by assuming that the first step of the interaction is metal ion insertion into a bond of the organic molecule. To be presented are ion cyclotron resonance spectrometry investigations of reactions of first row transition metal ions with a primary amine. They parallel the literature in that, for other types of organic molecules, selectivity in the insertion step is characteristic of the particular metal ion. An explanation of the reactivity trends of the first row transition metal ions is suggested based on the thermodynamics of the metal insertion process and on the metal electronic configurations which are conducive to formation of the reaction intermediate. Extended Hückel molecular orbital calculations are presented to support the bonding scheme for the reaction intermediate.

ACKNOWLEDGEMENTS

I would like to express my gratitude to my research advisors, Professors John Allison and James Harrison for their guidance, and to the Dow Chemical Company for their financial support of this work.

This thesis is dedicated to my parents Tom and Audrey Balistreri for their unending confidence, and most of all to my husband Michael whose patience and sense of humor made this possible.

TABLE OF CONTENTS

LIST OF TABLES

LIST OF FIGURES

CHAPTER I

ICR SPECTROMETRY

I. Ion Cyclotron Resonance Spectrometry Principles

A. Principles of ICR

The theory of ICR spectrometry has been thoroughly presented[1-5]. Important operating concepts are presented below.

Figure 1 is a block diagram showing the main components of the spectrometer system. Figure 2 is a diagram of the ICR cell which is situated in a magnetic field. Primary mass spectrometric functions occur in this cell: ions are formed in the source, and analyzed on their response to iscillating electric fields in the analyzer.

Since ions, formed by electron impact, are in a magnetic field, they experience a force at right angles to the velocity vectors which are perpendicular to the magnetic field. This velocity is due to the ion's thermal energy; $(\frac{1}{2})mv^2 = kT$. In terms of the reference axis in Figure 2, the magnetic field is in the z direction and, therefore, ions travel in a circular orbit in the xy plane. Since the system is in equilibrium, centrifugal force equals the magnetic force, and so the radius and frequency of orbit can be described as follows:

Centrifugal Force = Magnetic Force

$$\frac{mv^2}{R} = \frac{Q}{c} VB \qquad (1)$$

$$R = \frac{cmv}{QB}$$

$$w_c = \frac{V}{R} = \frac{QB}{MC} \qquad (2)$$

where:

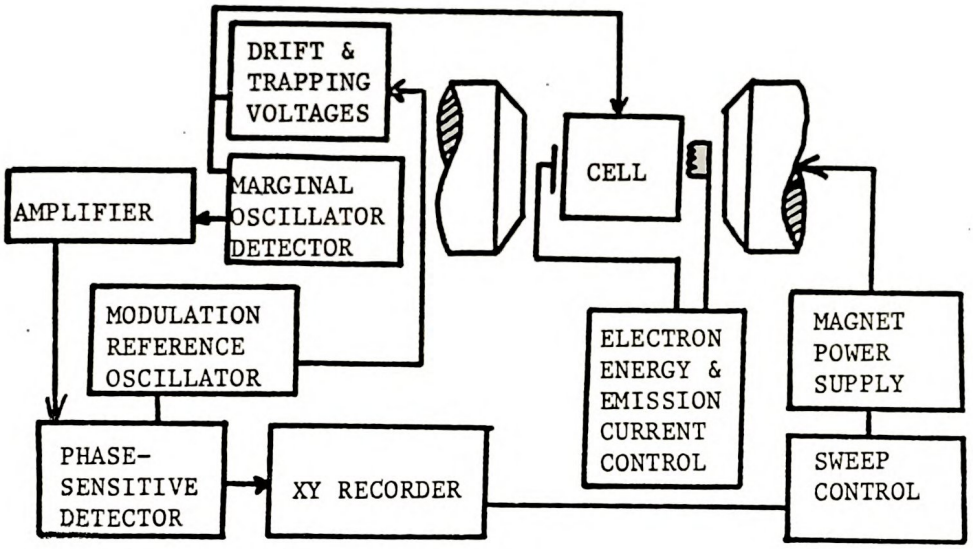

Figure 1. Block Diagram ICR Spectrometer

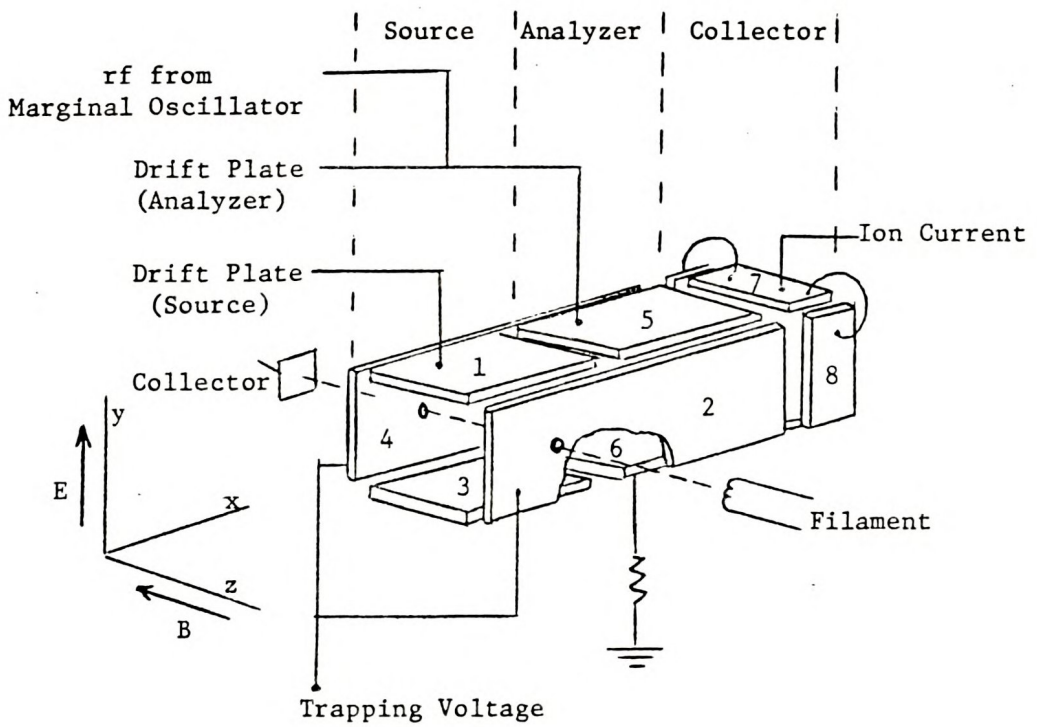

Figure 2. Diagram of ICR Cell

R= radius (meter)

C= speed of light

M = mass (AMU)

B = magnetic field strength (Tesla)

V = velocity (m/sec)

w_c = cyclotron frequency (sec^{-1})

Q = charge (coulombs)

To prevent ions from drifting to plates 2 and 4 and being annihilated, a trapping potential is applied. This creates a potential gradient of about .25 volt/cm from the center outwards to the plates. At thermal energies, this is a sufficient potential well for holding all ions in the center of the cell.

To move ions out of the source region, in the positive x direction, a voltage is applied across the top and bottom plates 1,5,3, and 6. In the electric field, the circulating ion accelerates when it goes with the field and decelerates when moving against it. Since the radius depends on velocity, the radius is different during different parts of the orbit. The net result is a cycloidal path, and a drift out of the source toward the collector. Detection is based on the ion's mass/charge ratio which is inversly proportional to the cyclotron frequency.

The marginal oscillator (m.o.) is a constant current device which provides oscillating electric fields across the top and bottom plates 5,6 in the cell. When an ion's cyclotron frequency matches the applied m.o. field's frequency the resistive impedance of the cell changes, and so the voltage to drive the current must change.

Detection is based on power absorption which is equivalent to a voltage change in the constant current generator.

$V = ixR$

$P = iV = (i)^2x(R)$

P = power

i = current

R = DC resistance, AC impedance

V = voltage

The sign of the voltage on the trapping plates 2,4 alternates at 20 Hz between +/+ and +/- so that the cell alternates between trapping and annihilating positive ions, respectively. The signal measured is the difference between peak-to-peak voltages in these two modes, as determined using a lock-in amplifier. The marginal oscillator frequency is usually set at 153 KHz so that 1 amu mass change is equal to 100 gauss (0.01 tesla).

Plates 7, 8 and 9, 10 at ground potential collect ions after they move through the cell. These plates are connected to an electrometer and are used to monitor total ion current.

ICR spectra are obtained by slowly varying the magnetic field with the detector operating at a constant RF frequency. A plot of power absorption vs. magnetic field gives a mass spectrum which is linear in mass.

The double resonance experiment assigns precursors to product ions so that reaction paths can be "unambiguously" determined. In a double resonance experiment the magnetic field is static so that the concentration of an ion of a single m/z (mass-to-charge) value in the analyzer can be monitored. At the same time, a second oscillator is connected to the source and its frequency varied. Just as in single resonance in the analyzer region, ions in the source absorb power when at resonance, increase their translational energy and radius of orbit, to a point where they are "ejected" from the cell. A drop in product ion intensity in the analyzer region indicates that a precursor has been ejected. Because the magnetic field strength is the same in both regions, equation (2) can be rearranged and solved for the identity of precursor ion in the source

when the double resonance oscillator frequency in the source is known:

$$B = \frac{(W_{product})(M_{product})(C)}{Q} = \frac{(W_{precursor})(M_{precursor})(C)}{Q} \quad (2)$$

or

$$M_{precursor} = \frac{W_{product}}{W_{precursor}} (M_{product}) \quad (3)$$

This technique implies a time frame for the ion-molecule reactions. If the reaction is so fast that products form in the source, or so slow that the precursor will be in the analyzer region, double resonance will not be successful. Also note that if $A^+ \longrightarrow B^+$, and $B^+ \longrightarrow C^+$, then both A^+ and B^+ will be determined as precursors of C^+. A more detailed discussion of this technique is in the literature[1,5-7].

B. Interpretation of Data for Metal Ion Studies

This thesis involves studies of organometallic ion/molecule reactions of the general type $M^+ + AB \longrightarrow$ products, where M^+ is a metal or metal containing species, and AB is an organic molecule. Some general points to be considered when interpreting ICR data for reactions of this type are given below[8].

1. Typical residence times in the spectrometer are on the order of milliseconds, which is about 3 orders of magnitude larger than those in a conventional mass spectrometer. At the usual experimental pressures of 10^{-5} torr, and this residence time, primarily single collision processes are observed.
2. Ions possess only thermal energy;

$$KE = (\tfrac{1}{2})(mv^2) = KT$$

In a conventional spectrometer ion kinetic energy is significantly increased by the high voltage repeller plates.

3. Reactions are assumed to have no activation energy.

4. Additional energy in the form of light or heat is not put into the system. Therefore only exothermic or thermoneutral reactions are observed. The total $\Delta H_{reaction}$ can be approximated by reactant and product heats of formation. Product ion energies are also a part of the energy balance but they cannot be measured. For an ion-molecule reaction of the type $M^+ + AB \rightarrow$ Products:

$$\text{Total Reaction Enthalpy} \approx \text{Energy In} - \text{Energy Back}$$

$$\approx \text{Energy to Break Bonds} - (\text{Energy to Form New Bonds} + \text{Product Kinetic Energies})$$

Using this type of analysis upper and lower limits on heats of formation and bond strengths can be estimated.

5. Bond strengths to highly coordinated (e.g. $Fe(CO)_n^+$) metal ions would be expected to differ somewhat from those of bare ions (e.g. Fe^+) since the amount of electron density available for bonding changes with the number and type of ligands.

CHAPTER II

ICR STUDIES OF TRANSITION METAL CHEMISTRY

II. ICR Studies of Transition Metal Chemistry

A. Overview and History

Transition metal chemistry has been studied extensively in solution and on bare metal and metal oxide surfaces. In the condensed phase, important factors affecting the chemistry are ligands and the solvent, which effect both the reaction energetics and properties of the metal center. Another factor which can be important in chemistry on surfaces is crystalline structure.

The study of the bare metal center by ICR spectrometry is relatively recent, dating back to only the early 1960's[9,10]. The atomic orbitals of a single metal center are different than the molecular orbitals of a coordination compound, or the band structure of a metal surface. Therefore, it would be reasonable to expect different chemistries for each of the three cases.

A useful tool for studying chemistry of isolated, bare transition metal ions is Ion Cyclotron Resonance (ICR) spectrometry. In an ICR experiment gas phase metal ions can be allowed to react with neutral organic molecules at relatively low pressures $\sim 10^{-5}$ to 10^{-6} torr. Under these conditions the simplest chemical event, the bimolecular collision, occurs.

The first mass spectrometric studies of transition metal containing molecules were on the fragmentation patterns of metal carbonyls[9,10]. Their volatilty allows for easy introduction into the mass spectrometer. Properties of these compounds are of general interest since they are prevalent in organometallic chemistry and catalysis.

Bimolecular reactions of metal ions with their neutral parent were first reported in 1964 by Schumacher and Taubenest who observed the formation of a dinickel complex from a nickel cyclopentadiene complex[11]. Bimetallic ions formed by ion/molecule reactions were also studied by Beauchamp in 1971 with $Fe(CO)_5$[12]. Muller in 1974 observed two types of reactions; formation

of small metal clusters (as did his predecessors), and ligand substitution reactions[13]. Beauchamp also reported reaction of ions formed by electron impact of $Fe(CO)_5$ with small molecules such as CH_3F, HCl, NH_3 and H_2O[12]. From these first investigations it became apparant that ICR studies could provide insights into metal-metal and metal-ligand chemistry, and thermodynamic information on bond strengths.

Ridge and co-workers were the first in 1976 to explain metal ion-neutral reactions as the formation of metal to carbon bonds by oxidative addition of the metal ion M^+, across the polar bond, C-A[14].

The M^+ insertion, β-H hydrogen shift mechanism has been thoroughly evaluated since the initial reports, and is now commonly accepted. In general terms the three steps of the mechanism are:

Oxidative Insertion into Polar Bond:

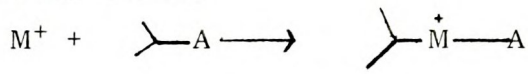

(4)

β-Hydrogen Shift:

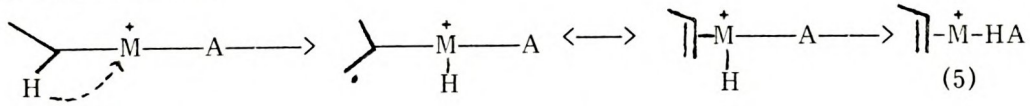

(5)

Competitive Ligand Loss:

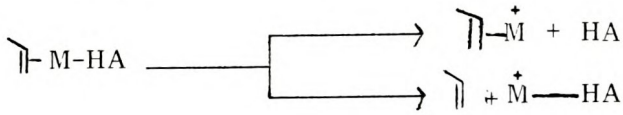

(6)

Representative examples of this chemistry are:

$$Ni^+ + C_2H_5I \longrightarrow NiI^+ + C_2H_5$$

$$Ti^+ + C_2H_6 \longrightarrow TiC_2H_4^+ + H_2$$

$$Fe^+ + C_3H_6 \longrightarrow FeC_2H_4^+ + CH_4$$

Gas phase chemistry generally differs from that in solutions. Rather than carbon-carbon bond formation, dehydrogenation and C-A bond breaking predominates[12].

The insertion/β-hydrogen shift/competitive ligand loss sequence is generally valid, but the specific reaction depends on the particular metal ion and on the organic substrate. A sufficient body of descriptive chemistry has been generated, enough to provide a first level approximation of reactivity trends. What follows is the summary of the chemistry of first row transition metal ions, organized by metal ion. The purpose is to indicate the overall level of activity of the metal ion by citing representative reactions. The most reactive metal ions are those which insert into the many different types of bonds; C-C, C-H and C-A where A is various oxygen, halogen, or nitrogen functionalities. In some cases the chemistry depends on the source of the metal ion. Volatilization/ionization techniques are discussed for these in context of their impact on the reaction path.

Two other types of experiments will be referenced since they provide structural and thermodynamic information about metal-ion/molecule reactions. Collision-Induced-Decomposition (CID) experiments explore structure of the (M^++substrate) species via their fragmentation patterns following collision with, eg., argon. Beauchamp and co-workers studied the thermodynamics of ion/molecule reactions. In their ion beam experiments the kinetic energy of M^+ is varied and the onset of different reaction paths is determined.

B. Summary of Reactions of First Row Metals

Titanium. Titanium reacts with saturated alkanes by inserting into both C-C and C-H bonds to eliminate small alkanes and hydrogen respectively. Of these two reactions, the preferred path is elimination of one or more hydrogens to create unsaturated ligands. The strong Lewis acid character of the Ti^+ ion was cited as the driving force for H_2 elimination[13].

The chemistry of the $TiCl_x^+$ ions (x = 0 to 4) has been characterized with small olefins[15]. The reactions precede with loss of H_2 or HCl depending on the value of x, or with loss at small olefins for substrates having more than 5 carbons.

In the gas phase chemistry of Ti^+ with halomethanes, alkyl chlorides, chloroethylenes and chlorobenzene, the predominant reaction was chloride transfer and oxidative halogen transfer to produce TiX^+ (where X = halide). Dehydrochloration of vinyl chloride resulted in formation of $TiCl_2(ligand)^+$. The possibility of endothermic reactions were raised in this study because the laser volatilization/ionization of titanium may have produced "hot" Ti^+ reactant ions.

The chemistry of Ti^+ with compounds containing C-O single and double bonds is characterized by the formation of TiO^+ and elimination of either a radical or alkene respectively. Much of the driving force for these reactions is the formation of the strong Ti^+-O bond. Reactions were not observed with carbonyl compounds having more than five carbons.

Chromium. The Cr^+ ion is relatively unreactive, and has not been characterized as well as some of the other first row transition metal ions.

Cr^+ can be produced by thermal decomposition of $CrCl_3$ on a hot rhenium surface, followed by surface ionization. This Cr^+ reacts with methane to yield CrH^+. In endothermic reactions with ethylene and cyclopropane it forms

$Cr-CH_2^+$. Beauchamps kinetic energy threshold analysis defines the chromium ion-carbene bond strength as 65 ± 7 kcal/mole.

The Cr^+ ion formed by electron impact on $Cr(CO)_6$ forms $Cr-CH_2^+$ in its reaction with methane, at thermal translational energies.

The above discrepancy is resolved by considering electronically excited states. If excited Cr^+ were formed by electron impact on $Cr(CO)_6$, the thermodynamic analysis of the reaction assuming reactants in their ground states would yield incorrect results. Electronically excited Cr^+ has been involved in other reactions. Ridge et al.[18] suggests that two Cr^+ species are formed on electron impact of $Cr(CO)_6$. The state which reacts slowly with $Cr(CO)_6$ is twice as abundant as the rapidly reacting state. Other studies have focussed on the types of species produced by electron impact on $Cr(CO)_6$, but are not in agreement[20,21].

In his analysis of the reaction of Cr^+ with butane Ridge found products indicative of insertion only into the weakest C-C bond, and that hydrogen elimination dominated. The CID spectra of these ion/molecule complexes yielded mainly the Cr^+ fragment. Although these species were formed from $Cr(CO)^+$ and not Cr^+, the results suggests that the neutral organic retains its integrity and that "Cr^+" does not directly insert into the bond.

The chemistry with compounds containing C-O bonds is greatly influenced by the strong Cr^+-O interaction[15]. The product of Cr^+ reaction with diethylether, $CrC_2H_4O^+$ was explained by the metal insertion, β-H shift mechanism. In its reaction with polyethers small ligands were formed with a total of more than one oxygen to one Cr^+ ion. The chemistry with crown ethers also produced ions with high O:Cr ratios.

Manganese. ICR spectrometry has characterized reactions of both Mn^+ and Mn_2^+ since both are major ions from electron impact on $Mn_2(CO)_{10}$.

Both Mn^+ and Mn_2^+ are completely unreactive with saturated alkanes[23,47]. The carbene $Mn\text{-}CH_2^+$ can be formed from ethylene oxide or cyclopropane. If the oxide MnO^+ is formed by reaction of Mn^+ with NO, then the metal carbene can be produced from ethylene[19].

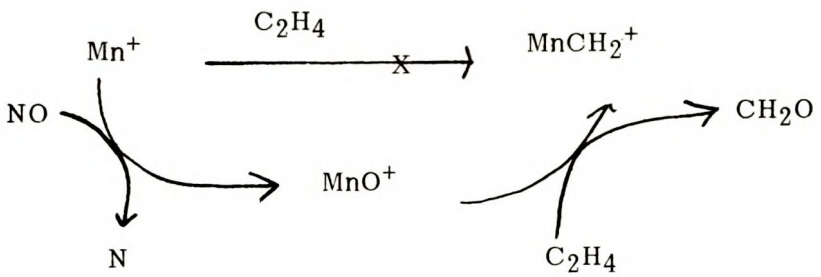

These reactions yield a bond strength for $Mn^+\text{-}CH_2$ of about 92 to 100 kcal/mole. This can be considered to be a very strong bond. The Mn^+ ions for these experiments were produced by 100 eV electron impact ionization of $Mn_2(CO)_{10}$. Excited states of reactant ion Mn^+ were dismissed because appearance potential curves for $MnCH_2^+$ from cyclopropane matches that of Mn^+.

Both Mn^+ and Mn_2^+ form the bromide, $M^+\text{-}Br$, in their reactions with alkyl bromides. Mn_2^+ but not Mn^+ will dehydrohalogenate alkyl halides. Mn_2^+ will also lose an Mn atom to form the $Mn^+\text{-}RX$ adduct in its reactions with alkyl halides (RX). Those reactions with alkyl halides have been explained as occurring by interaction with only one end of the halide rather than insertion into the C-halide bond[23].

The Mn_2^+ cluster is of interest because it has an electron configuration between Mn_2 and Cr_2[22]. These dimers result, primarily, from 4s σ bonding:

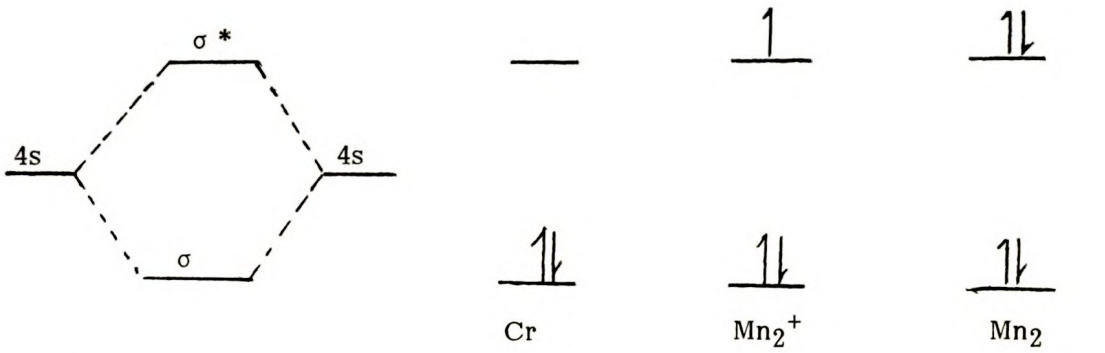

	Cr	Mn_2^+	Mn_2
Bond Order	1	0.5	0
Bond Strength	1.56 eV	0.85 eV	0.33 eV

Copper. Copper ions are produced for gas phase studies by laser volatilization/ionization since stable, volatile copper carbonyls do not exist. Freiser evaluated Cu^+ as a chemical ionization reagent with a series of oxygenated compounds[24]. Definite reactivity trends were identified and explained as dissociative attachment of Cu^+ to the substrate followed by hydrogen migration and dissociation. Products of neutral insertion into the C-OH bond of alcohols were not observed. Freiser concluded that none of the reactions uniquiocally required initial metal ion insertion into the bond. However, the metal insertion/ β-hydrogen shift/ligand loss mechanism is consistent with reaction products.

Similarly, Staley's report of reaction of Cu^+ with alkyl chlorides were explained as initial association of Cu^+ at the chloride site followed by halide transfer and loss of R^+. These results did not provide any direct evidence for insertion into C-Cl bonds[25]. For both Freiser's and Staley's studies, kinetically hot Cu^+ were suggested as possible reactive species. Freiser also did clustering

reactions and found that the coordination complexes which were formed had a close correspondance to those which are formed in solution[76].

Iron, Cobalt, Nickel. The group 8 metal ions have very similar gas phase chemistry with most compounds[26-42]. With alkanes having more than 3 carbons, Fe^+, Co^+ and Ni^+ all insert into internal C-C bonds to form olefin complexes. Fe^+ also inserts into the stronger terminal C-C bond and C-H bonds. Co^+ and Ni^+ are selective against insertion into the terminal C-C bond[28,29,31-34]. Collision induced decomposition spectra of metal containing products indicate that primary β-hydride transfer is more facile than secondary for Fe^+, while the reverse is true for Co^+ and Ni^+[28]. All three decarbonylate cyclopentanone, but again Fe^+ shows less selectivity also eliminating both H_2 and C_4H_8[28].

A recent article by Freiser reports that FeO^+ is more reactive with saturated alkanes than Fe^+. This was attributed to the thermodynamically more favorable loss of H_2O than simple hydrogen elimination[40].

In their reactions with alkyl halides (RX) and alcohols (ROH), the ions were observed to insert into the polar RX and ROH bonds. Ni^+ was postulated to have a higher affinity for halogens since it formed primarily NiX^+ and the other two formed mainly FeR^+ and CoR^+[30].

In a comparison of proton affinities of first row transition metals, Beauchamp identified periodic trends, and noted that the bond energy depends heavily on geometry and orbital hybridization. Of all the carbonyls, iron pentacarbonyl has the greatest bond strength[26].

Zinc. Little information is available on the gas phase chemistry of Zn^+. One reaction which has been characterized is proton transfer as a function of ion kinetic energies with the zinc atom. Proton transfer results in the ionized zinc species-ZnH^+. Comparison of low energy and high energy sources of RH^+ indicate that the rate depended on internal and kinetic energies of reactants

and that the mechanism involved formation of an excited state of ZnH^+. The only reaction reported with protonated alkyls was charge and proton transfer[43].

C. Summary of Reactivity Trends

In a very few words, the above can be summarized:

1. Ti^+ and Fe^+ are the most reactive first row metal ions. Their reactions produce ions and neutrals characteristic of insertion into C-H, C-C and polar bonds of alkyl halides and oxygen containing compounds.
2. Ni^+ and Co^+ are the second most reactive. Products of their reactions indicate discrimination between bonds based on bond strength. They tend to insert into weaker bonds.
3. Cr^+ and Cu^+ rank about third in reactivity. Analysis of their reactions indicate that they often may not insert into bonds but may interact by "outer sphere" mechanisms.
4. Mn^+ and Zn^+ are usually unreactive.
5. Sc^+ and V^+ have not been characterized.

If the above relative activities were scaled and plotted against atomic number, an interesting plot results:

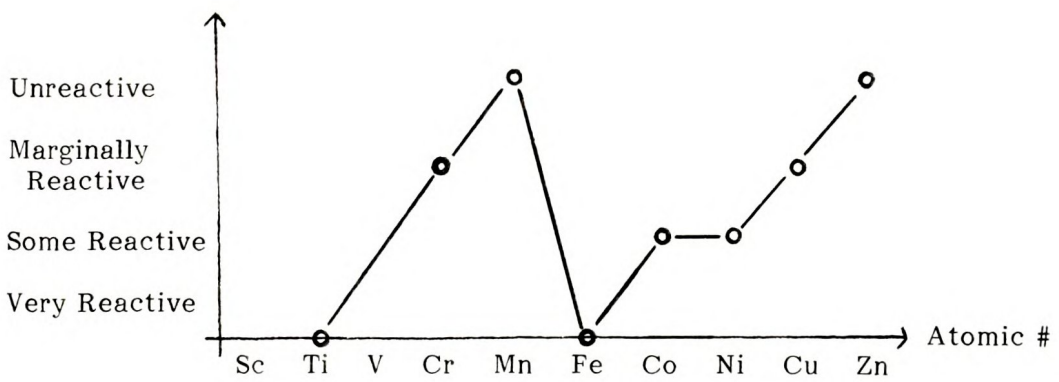

This plot resembles a typical plot of any given periodic property of transition metals. In this case, level of reactivity with hydrocarbons is plotted instead of the usual properties such as ionization potential, atomic or ionic radius, electronegativity, electron affinity, and others. Periodic nature is generally attributed to filling the oribitals (d orbitals in this case), and the extra stability of half and totally filled orbitals. That is, these properties are a function of electronic configuration.

In transition metal chemistry, electronic configuration is used frequently to pattern trends in geometry and reactivity. Best stated by J.K. Burdett in his text on theoretical models in inorganic chemistry; "...very often molecular properties may be rationalized purely on the basis of electronic configuration rather than the exact nature of the metal and the ligands"[44].

Some examples of the utility of explaining trends with electronic configurations are: 1) Extra stability is associated with compounds of noble gas configuration; 2) Geometry is related to the d^n configuration; 3) Simple crystal field theory predicts magnetic and spectral properties; 4) The Jahn-Teller Theorem predicts the consequences of degenerate d orbitals; and 5) Reactivity is related to configuration. Octahedral d^6 species have a saturated coordination sphere and undergo reductive elimination rather than oxidative addtion. Good choices for the latter reaction are unsaturated d^3 and four coordinated d^{10} species[45].

Bonding is also discussed in terms of configuration. d electrons of coordination compounds must first pair up in order to free orbitals for bond formation. For example, the 4s electron must be promoted to the 3d orbital in order to be occupied by the incoming ligand. Conversely, the sigma bond in organometallics is made by pairing odd electrons of the organic radical and the metal. In either event, dative or sigma bond, the metal must obtain a

suitable electronic configuration in order to form a bond. If the ground state configuration is not conducive to bond formation, an excited state of the metal must first be formed:

$$M \xrightarrow[+\text{ "Promotion Energy"}]{\text{Rearrange}} M^* \xrightarrow[+R\cdot \text{ or } R:]{\text{Form Bond}} M\text{-}R$$

ground state	excited state bonding configuration	Bonded Species

These ideas are the same as hybridization theory for main group elements. Were it not for the formation of the carbon $2s^1 2p^3$ excited state, there would not be tetrahedral geometry for carbon. The energy required to form the excited state can be manifested in several ways. For example, the bond angle of Group VA and VIA hydrides decreases as the central atom "hybridization energy" increases. Another example is the difference in the strength of the two C-O bonds in CO_2. The energy required to break the first and second bonds is 127 kcal/mole and 256 kcal/mole, respectively. The weakness of the first bond has been attributed to the greater "promotion" or "hybridization" energy in comparison to the remaining bond. This energy reduces the overall thermodynamic bond strength which is that measured experimentally[46].

The past utility of considering contributions due to electronic configuration can not be denied. The purpose of this thesis is to explore the extent of influences of electronic configuration on the chemistry of a very simple transiton metal species - the bare M^+ ion. Further, if electronic configuration is a significant factor, can it be used to predict trends in M^+ chemistry?

The existing data base of bond strengths of first row transition metal ions to organic species such as CH_3, H, CH_2, O suggests two correlations. First, for R=CH_3, H, CH_2, Fe^+-R bonds are stronger than Co^+-R or Ni^+-R bonds. Second, for all metal ions: M^+-H < M^+-CH_3 < M^+-CH_2.

Table 1. Metal-Ligand Bond Dissociation Energies kcal/mole

	Cr^+-R	Mn^+-R	Fe^+-R	Co^+-R	Ni^+-R	Zn^+-R
R = H	35 ± 4	53 ± 3[c]	58 ± 5	52 ± 4	43 ± 2	60[d]
R = CH_3	37 ± 7	71 ± 7[c]	68 ± 4	61 ± 4	48 ± 5	67 ± 1[e]
R = CH_2	65 ± 7	94 ± 7	96 ± 5	85 ± 7	86 ± 6	
R = O	77 ± 5	57 ± 3	68 ± 3	65 ± 3	45 ± 4	
promotion energy	34.2	0	0	9	24.0	0

In 1981 Beauchamp et al.[47] first reported a correlation between these metal ion-ligand bond energies and electronic configuration of the metal ion. For first row transition metals there is a linear relationship between the energy of the lowest $3d^{n-1}4s$ configuration and the M^+-R bond strength for R=H and R=CH_3 (see figure below). This suggests that the metal-ligand bond involves primarily the 4s orbital of the metal. The conclusion is in agreement with theoretical studies of bonding of first row metal hydrides[3]. The correlation does not hold for carbenes and oxides, presumably because there is substantial π character to these, at least for some M^+.

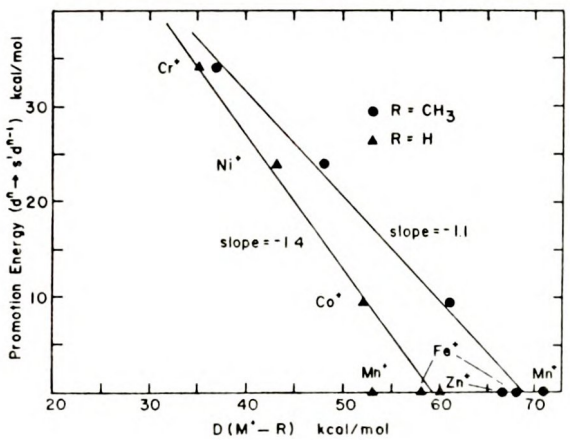

A single metal configuration could not describe this bonding. The correlation also does not hold for the second row group 8 metal ions Rh^+ and Pd^+, which indicates that the $4d^{n-1}5s^1$ configuration is not important and that the bonding is predominately through the metal's 4d orbitals.

Thermodynamics also relates to the selectivity as well as the reactivity trends previously mentioned. The Fe^+ ion which forms the strongest bonds, is indiscriminate for insertion into C-C versus C-H bonds which differ by about 20 kcal/mole. The Ni^+ ion is much more selective as indicated by branching ratios of reactions with alkanes. Co^+ ranks between these two. This ranking

matches precisely the ranking of the metal ion bond strengths. The two first row transition ions with largest promotion energies, Cr^+ at 34.2 kcal/mole and Cu^+ at 63 kcal/mole, are only mildly reactive[47]. However, the lack of reactivity of Mn^+ and Zn^+ cannot be similarly explained. Therefore the data in Beauchamps table cannot be used to predict reactivity of M^+. Note that the metal ion reactions usually proceed via M^+ insertion into a bond and that this requires formation of two bonds to the metal.

Periodic trends were also noted in proton affinities of organo-transition metal complexes, where protonation occurs at the metal center. Of the first row transition metal carbonyls, the maximum proton affinity is for $Fe(CO)_5$, which is the most reactive ion[26].

Carbonyl	Bond Energy $D(B^+-H)$ kcal/mole
$V(CO)_6$	56 ± 3
$Cr(CO)_6$	58 ± 3
$Mn(CO)_5(CH_3)$	67 ± 3
$Fe(CO)_5$	74 ± 5
$Ni(CO)_4$	62 ± 3

It also was noted that the homologous second row compounds had a stronger bond.

Most recently, a series of papers have been published concerning periodic trends for metal ions produced by a sparked discharge[48-52]. Those experiments differ from the ICR experiment because resulting metal species have a significant kinetic energy and are not in their ground states. Even though the plasma-like experimental design makes correlations limited, Bursey et

al. suggest reactivity trends. They proposed that reaction of fourth period elements with propane and propene was by metal ion insertion into the C-C bond and that the 4s orbital was responsible for the reaction. Reactivity trends were rationalized on this basis, and a correlation was found between product ion intensity and the inverse of promotion energy to the lowest lying $3d^n4s^1$ state. The 4p orbitals are not needed for bonding in this scheme[48]. Reactivity of copper ions towards oxygenated compounds is greater for the ions produced by a spark than for laser ionized copper in ICR studies. More fragmentation of the original ion-molecule complex was also found. Both effects are attributed to excited states which are capable of bonding[50]. However, these experiments yield very unpresidented results. The current explanations of reactivity are high speculative.

D. The Amine Anomaly

One major anomaly of gas phase metal ion-organic molecule chemistry is the reaction of Co^+ with primary and secondary amines. Co^+ has been characterized with a wide variety of organic compounds and has exhibited the predicted reactions:

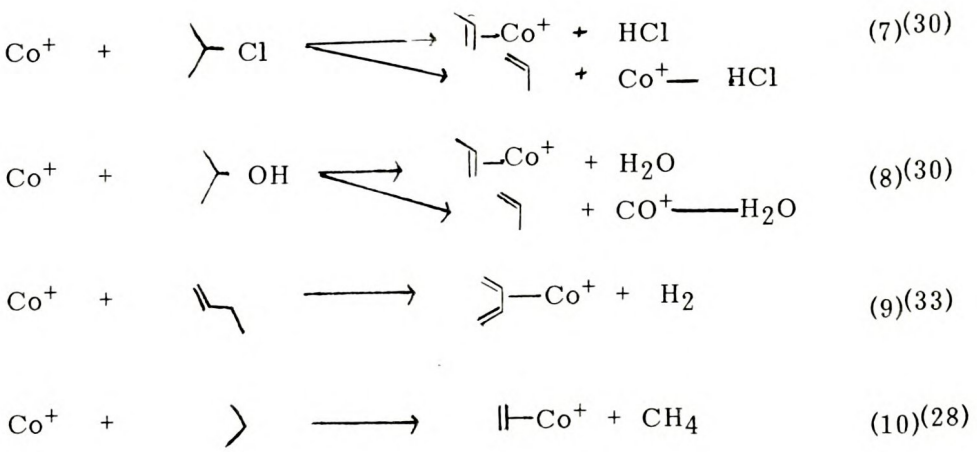

However, reaction with the amine is characteristic of a saturated alkane. That is, the expected insertion into the C-NH_2 bond does not occur.

$$Co^+ + C_3H_7\text{-}NH_2 \not\longrightarrow Co\text{-}NH_3^+ + C_3H_6$$
$$\longrightarrow Co\text{-}\!\!\nearrow^{+} + NH_3$$

This unusual behavior was studied by Radecki and Allison. The chemistry of Co^+ with primary, secondary and tertiary amines was reported. Analysis of the chemistry is given below[53].

Consider first the overall thermodynamics of the NH_3 elimination reaction, using n-propyl amine as the representative amine:

$$Co^+ + C_3H_7NH_2 \longrightarrow Co(C_3H_6)^+ + NH_3$$

The total energy of the reaction is the difference between the energy to rearrange the organic molecule and the energy to form the metal-ligand bonds. The energy of rearrangement is the difference between the free energy of formation of ligands and the starting amine.

$$C_3H_7NH_2 \longrightarrow C_3H_6 + NH_3$$

$$-18.5 \frac{\text{kcal}}{\text{mole}} \qquad +4.88 \frac{\text{kcal}}{\text{mole}} \quad -11.0 \frac{\text{kcal}}{\text{mole}}$$

Energy required = + 12.36 kcal/mole

For the reaction to be exothermic, the "energy back", the cobalt-propene bond strength, must be greater than 12.36 kcal/mole.

Fortunately, cobalt ion chemistry has been characterized for other compounds, and so a number of cobalt-ion-bond strengths to various ligands are available.

Bond	Bondstrength (kcal/mole)
Co^+—H	52 ± 4
Co^+—CH_3	61 ± 4
Co^+—CH_2	85 ± 7
Co^+—OH	71 ± 5

This suggests that the cobalt binds strongly to many ligands, of both sigma and sigma/pi bonding and that the cobalt ion-propene bond should fullfill the 12.36 kcal/mole requirements.

An estimate of the Co^+-propene bond strength is provided by the reaction of cobalt ion with 2-propanol:

$$Co^+ + C_3H_7OH \longrightarrow Co^+\text{-}C_3H_6 + H_2O$$

This reaction provides a lower limit of 12.68 kcal/mole for $D(Co^+\text{-}C_3H_6)$, and therefore predicts the Co^+-n-propylamine reaction to be exothermic.

An example calculation is given below:

Co^+ with isopropyl alcohol

Energy In: $C_3H_7OH \longrightarrow C_3H_6 + H_2O$

-65.6 kcal/mole +4.88 -57.8

Energy Back: $Co^+ + C_3H_6 \longrightarrow Co^+\text{-}C_3H_6$

Total Energy = Energy In - Energy Back

(-) = +12.68 kcal/mole - $D(Co^+-C_3H_6)$

12.68 kcal/mole < $D(Co^+-C_3H_6)$

Co^+ with isopropyl amine

Energy In = $C_3H_7NH_2 \longrightarrow C_3H_6 + NH_3$

-18.5 kcal/mole +4.88 -11

Energy In = 12.36 kcal/mole

Therefore, If reaction with $C_3H_7NH_2$ is exothermic then 12.36 kcal/mole < $D(Co^+-C_3H_6)$

Since the thermodynamics of the overall reaction are favorable, one mechanistic step must be rate limiting. In the first step, if the metal ion preferentially inserts into the weakest bond of n-propyl amine, attack at the carbon-nitrogen bond would be expected.

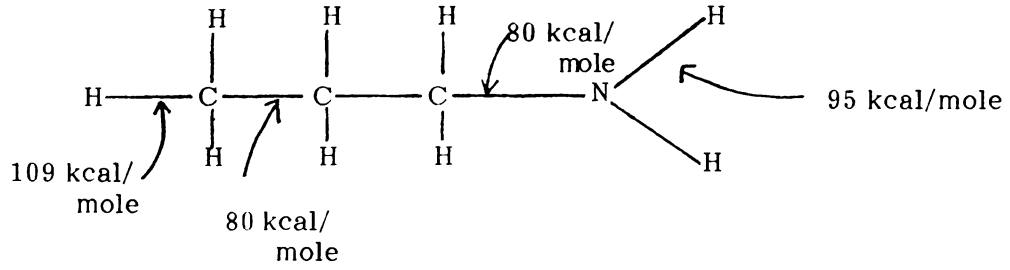

Below are the insertion reactions and resulting products listed from most to least likely to occur based on the strength of the organic bond.

	Bond	Products
1st	C-NH_2	$Co(C_3H_6)^+ + NH_3$
		$Co(NH_3)^+ + C_3H_6$
2nd	C-C	$Co(CH_3NH_2)^+ + C_2H_4$
		$Co(C_2H_4)^+ + CH_3NH_2$
3rd	N-H	$Co(C_3H_5NH_2)^+ + H_2$
		$Co(H_2)^+ + C_3H_5NH_2$
4th	C-H	$Co(C_3H_5NH_2)^+ + H_2$
		$Co(H_2)^+ + C_3H_5NH_2$

The reaction which is most likely to occur does not. According to the Arrhenius equation, KT = A exp($-E_a/RT$), kinetics have both geometric (A) and thermodynamic (E_a) aspects. Thermodynamics of the metal ion insertion reaction are described:

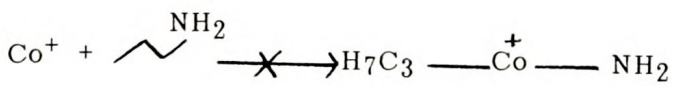

$$C\text{-}NH_2 = 80 \text{ kcal/mole}$$

$$Co^+\text{-}C_3H_7 \gtrless Co^+\text{-}CH_3 = 61 \pm 4 \text{ kcal/mole}$$

This places an upper limit on the $C_3H_7Co^+$-NH_2 bond at 19 kcal/mole. This low a bond strength would certainly be an anomaly It is more than 30 kcal/mole weaker than the weakest, the Co^+-H bond. The second possibility is that the encounter geometry is not favorable. Several facts, however, make this seem unlikely. Analogous reactions with saturated hydrocarbons are facile.

The cobalt ion also inserts into the carbon-nitrogen bond of tertiary amines and into other C-N bonds like $C-NO_2$[92]. Using ethyl as the model alkyl group, Table 2 below shows that the higher C-N bond strength of tertiary amine places tougher requirements on the cobalt ion-amide bond. Yet, the insertion occurs only with the tertiary amine. From this it can be concluded that the substitutent on the amide group greatly effects the bond, and that geometry is not the controlling factor in metal ion insertion.

Table 2. Reactivity of Amines with Co^+

AMINE	C——N BOND STRENGTH	OBSERVATION: INSERT INTO C——N ?	IMPLICATION: Co^+——NR_2 BOND STRENGTH
$(C_2H_5)NH_2$	77 KCAL/MOLE	NO	< 19 KCAL/MOLE
$(C_2H_5)_2NH$	↓	NO	↓
$(C_2H_5)_3N$	89 KCAL/MOLE	YES	> 59 KCAL/MOLE

The second step of the reaction following M^+ insertion is a β-hydrogen shift. Again the well developed chemistry of cobalt indicates that it is facile and has been observed for many classes of compounds. Therefore, the β-hydrogen shift will be assumed to be facile.

Competitive ligand loss is the third possible bottleneck of the reaction. Loss of a neutral must occur for any information to be extracted in the ICR experiment, since identification of products is based solely on mass-to-charge ratio. For example, both the simple coordination compound $Co(C_3H_7NH_2)^+$ and the intermediate (I) would have the same ratio of 118. The former suggests that Co^+ cannot insert into the carbon nitrogen bond, the latter does not. Additional mass spectroscopic techniques, such as Collision Induced Dissociation must be used to distinguish between the simple cobalt-amine adduct and the intermediate(I).

The above can be depicted by the following reaction diagram. The entire reaction is thermodymically "downhill". The β-hydrogen shift and competitive ligand loss steps appear to have little activation energies. Insertion into the carbon-nitrogen bond is proposed to be rate-limiting due to the thermodynamics of metal-ion insertion. Further, this is proposed to be due to the anomalously weak Co^+-NH_2 bond which appears to be less than 19 kcal/mole.

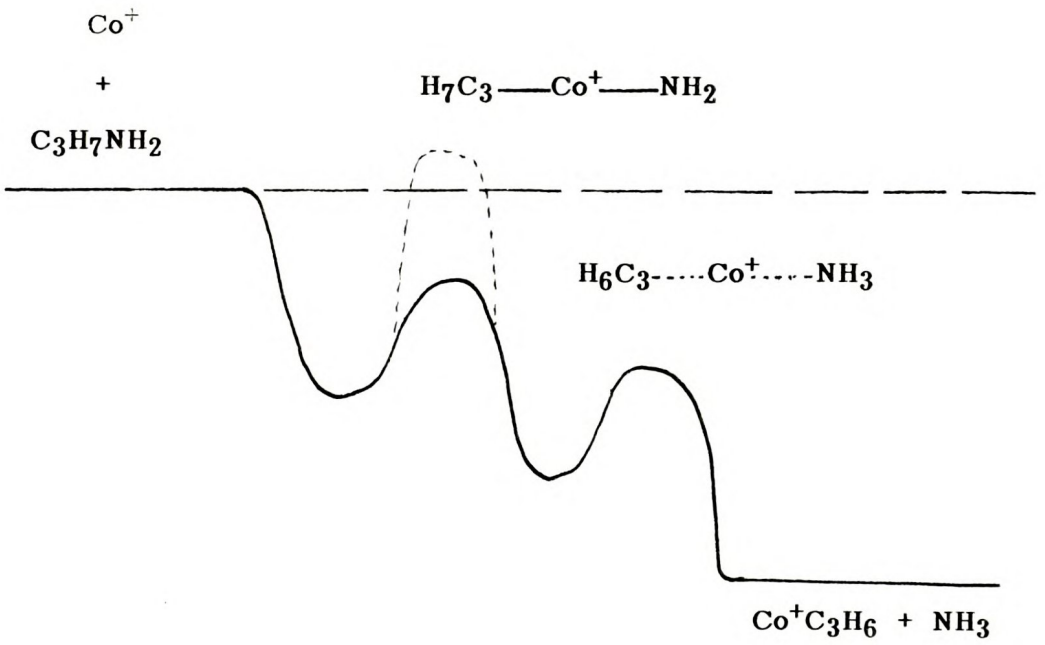

E. Purpose of this M^+-Amine Study

The unusual behavior of Co^+ with amines raises some interesting questions:

1. Would other first row transition metal ions react with amines to give products which also suggest metal amine bond strengths as weak as Co^+-NH_2? It has been shown that for most M^+-R, the bond strengths generally correlate with the metal ion; and that Co^+ has neither the weakest or strongest bonds.
2. If the M^+-NH_2 bonds are similarly weak, is this related to any unusual feature of NH_2, or does this relate to some property of the metal - such as electronic configuration, or <u>both</u>?

To answer these questions, the chemistry of six first row transition metal ions Cr^+, Mn^+, Fe^+, Ni^+, Cu^+, and Zn^+ and the dimer ion Mn_2^+, with a representative amine - n-propyl amine, was studied.

CHAPTER III

TRANSITION METAL AMIDES IN THE CONDENSED PHASE

III. Transition Metal Amides in the Condensed Phase

There are two interesting points pertaining to the occurance of first row transition metal amides: 1) primary amides have never been isolated; 2) of secondary and tertiary amides, fewer stable compounds exist for the later metals.

There are several possibilities or explanations offered for this. Pi bonding is suggested by the planarity of the amides, and the short metal-nitrogen bond lengths. A pi contribution would be reduced in later metals because the more full d orbitals are less likely to accept electron density from nitrogen. The lower energy barrier to inversion at the nitrogen makes the importance of this factor questionable. It has more recently become apparent and generally accepted that steric effects play a major role. Use of bulky ligands has led to isolation of complexes with very low coordination numbers, such as $Co[N(SiMe_3)_2]_2$. The reason for this is the kinetic stabilization offered by these ligands. The larger the group, the more difficult the condensation process to product NH_3, NH_2R or NR_3.

To summarize, the geometry of amides is typically planer due to pi bonding. The stability of these compounds, however, is primarily determined by kinetics of the reaction to eliminate NR_3. Therefore, primary amines are kinetically unstable.

CHAPTER IV

RESULTS AND DISCUSSION

IV. Results and Discussion

A. Experimental

All experiments were performed on an ion cyclotron resonance spectrometer operating in the drift mode using trapping voltage modulation and phase sensitive detection. The instrument is of conventional design and was built at Michigan State University. The ICR cell is situated in the 1.5" gap between the polecap's of a Varian 12" electromagnet which is controlled by a Varian V-7800, 13 kW power supply and a Fieldial Mark I magnetic field regulator. The cell is 0.88" x 0.88" x 6.25". 70 eV electrons are used for ionization. A Wavetek Model 144 sweep generator is the secondary oscillator used to identify precursors of products in double resonance experiments.

The ICR cell is housed in a stainless steel vacuum system which is pumped by a 4" diffusion pump with a liquid nitrogen cold trap and an ULTEK 20 L/S ion pump. Samples are admitted by Varian 951-5106 precision leak valves. Approximate system pressures are measured by a Veeco RG 1000 ionization gauge.

Data were acquired as follows. First the electron impact products of metal containing compounds alone were determined. Spectra up to mass 220 were obtained at both low (5×10^{-6} torr) and high (1×10^{-5} torr) pressures. Ions unique to high pressure spectra are the result of ion/molecule reactions. Double resonance was performed on these and on major ions in low pressure spectra. The system was then evacuated to a base pressure at 10^{-7} torr, and the process repeated for the amine. Such mass spectral analyses of each reactant, separately, allowed for the determination of: 1) ion/molecule reactions in the single component system, and 2) purity of each compound.

Finally a mixture of the two (organic and organometallic) is introduced into the cell at a 1:1 ratio and a total pressure of 1×10^{-5} torr. Ions not present

in the previous cases are assumed to result from ion/molecule reactions from ions of one compound with the other neutral compound. Double resonance was performed on all product ions. In some cases the ratios of organic to organometallic were adjusted to facilitate determination of precursors. In other cases the system pressure did not stabilize due to neutral-neutral reactions. Data reported represent the best attempt at a 1:1 ratio and a total pressure of 1×10^{-5} torr. Significant deviations will be noted.

The n-propyl amine was obtained from Aldrich Chemical Co. Sources of the metal ions, and their suppliers are given below:

$Cr(CO)_6$ - Alfa Chemical Co.

$Mn_2(CO)_{10}$ - Alfa Chemical Co.

$Fe(CO)_5$ - Aldrich Chemical Co.

$Ni(CO)_4$ - Alfa Chemical Co.

$Ni(PF_3)_4$ - Alfa Chemical Co.

$Cu(CF_3COCH_2COCF_3)_2$ - Research Organic/Inorganic Chemical Inc.

$Zn(C_2H_5)_2$ - Alfa Chemical Co.

The anhydrous form of copper bishexafluoroacetylacetonate was obtained by slow dehydration of the dihydrate in vacuo over fuming sulfuric acid in a dessicant container. All samples were degassed by three freeze pump thaw cycles. After degassing the vapor of the liquid samples which typically is a vapor pressure of about 4 torr, is admitted to an evacuated glass bulb. Sample bulbs are attached to the spectrometer by a two-sample inlet system. The three solids; $Cr(CO)_6$, $Mn_2(CO)_{10}$, and $Cu(acac)_2$ were gently warmed to raise their vapor pressure. The vapor pressure of $Zn(C_2H_5)_2$ is sufficiently high that it does not need to be heated in order to achieve adequate pressure in the ICR.

B. Results

Table 3 lists all the products of reaction between $C_3H_7NH_2$ and ions formed by electron impact on the organometallic compounds. Tables 4 and 5 are similar listings for products of reaction of M^+ and ML^+ respectively. To indicate overall level of activity, product ion intensities are relative to M^+ at 100%.

If only M^+ and ML^+ reacted to produce ions, the number in Tables 4 and 5 would sum to the total ion intensity in Table 3. This is usually not the case. Values in Tables 4 and 5 are the product of ion intensity (Table 3) and double resonance fraction of precursor M^+ and ML^+. Ions other than M^+ and ML^+ were precursors and therefore intensities do not sum up as expected. For example Mn_2^+ would give Mn-R^+ products; $Ni(PF_3)_2^+$ was the only precursor to $Ni(PF_3)(NH_2)^+$, and in some cases the metal amine adduct ($M{\cdot}C_3H_7NH_2^+$) was a precursor. (Also, the m/z = 30 ion, CH_2NH_2 was frequently a major precursor).The interest here is not to explore all reaction pathways, so these precursors are not dealt with in detail.

Table 6 lists the reactions by groupings which are referred to in Table 3, 4 and 5. This will suggest neutrals eliminated in formation of the product ion. Table 7 lists branching ratio's for most reaction systems, $Fe(CO)_5$, $Ni(CO)_4$, and $Ni(PF_3)_4$.

The copper-amine system behaved differently than all others. The system pressure of the mixture would not stabilize at any pressure or any ratio of amine to metal. Alone, each component was capable of sustaining constant pressure; the problem was only with the mixture. Product ion intensities are proportional to the ratio of components and to total pressure. Therefore, the data in Tables 3,4, and 5 are the best approximation of intensity at 1×10^{-5} torr.

Masses of major product ions in the mixture did not fit any that would

Table 3. Products of reaction of n-Propyl Amine with Products from Electron Impact on the Metal Source *

		Cr^+	Mn^+	Mn_2^+	Fe^+	Ni^{+a}	Ni^{+b}	Cu^+	Zn^+
	Product Ion								
I	$M(NH_3)^+$				7				
	$M(L)(NH_3)^+$				7				
	$M(L)_2(NH_3)^+$				3				
	$MA(NH_3)^+$				3				
	$M(L)(NH_3)^+$				3				
	$M(C_2H_5NH_2)(NH_3)^+$				3				
	$ML(NH_2)^+$						2		
II	$M(C_3H_6)^+$				4				
III	$M(C_2H_5N)^+$				5				
	$M(C_3H_7N)^+$	3			4				
	$M(A)(C_3H_7N)^+$	7							
IV	$M(CH_3NH_2)^+$				23	25	24		
	$M(C_2H_5NH_2)^+$				7	6			
	$M(L)(CH_3NH_2)^+$						9		
V	MA^+	31	34	6	129	19	30	100	
	MLA^+	2		10	5	23	25		86
	ML_2A^+				3				
	MA_2^+	4	8		7	19	27	110	
	MLA_2^+		2						

a = $Ni(CO)_4$ b = $Ni(PF_3)_4$
L = Ligand A = Amine $C_3H_7NH_2$

*Ion intensities are relative to M^+ at 100%.

Table 4. Products of Reaction of M^+ with n-Propylamine (Intensity Relative to M^+ = 100%)

	L	Cr^+ CO	Mn^+ CO	Mn_2^+ CO	Fe^+ CO	Ni^+ CO	Ni^+ PF_3	Cu^+ hfa	Zn^+ C_2H_5
	Product Ion								
I	$M(NH_3)^+$				3.5				
	$M(A)(NH_3)^+$				3				
	$M(A)_2(NH_3)^+$				3				
II	$M(C_3H_6)^+$				1				
III	$M(C_2H_5N)^+$				2				
	$M(C_3H_7N)^+$				1				
IV	$M(CH_3NH_2)^+$				23	16			
	$M(C_2H_5NH_2)^+$				7				
V	$M(A)^+$	31	34	16	18	30	71		
	$M(A)_2^+$	4	8	7					
	$M(L)(A)^+$					4			

A = Amine $C_3H_7NH_2$
L = Ligand hfa = hexafluoroacetylacetonate

Table 5. Products of Reaction of ML^+ with n-Propyl Amine (Intensity relative to M^+ = 100%)

	L	Cr^+ CO	Mn^+ CO	Mn_2^+ CO	Fe^+ CO	Ni^+ CO	Ni^+ PF_3	Cu^+ hfa	Zn^+ C_2H_5
	Product Ion								
I	$M(NH_3)^+$				3.5				
	$M(L)(NH_3)^+$				3.5				
	$M(L)(A)(NH_3)^+$				3				
	$M(L)(NH_2)^+$						2		
II	$M(C_3H_6)^+$				3				
III	$M(CH_3NH_2)^+$						24		
	$M(C_2H_5N)^+$				3				
	$M(C_3H_7N)^+$				3				
IV	$M(CH_3NH_2)^+$						24		
	$M(C_2H_5NH_2)^+$					6			
	$M(L)(CH_3NH_2)^+$						9		
V	M(A)		34		65	8			
	$M(A)_2^+$		8		7	19			
	$M(L)(A)^+$	2		10	5	23	25		
	$M(L)(A)_2^+$	4	2		3			36	16
	$M(L)_2(A)^+$								

A = Amine $C_3H_7NH_2$ hfa = hexafluoroacetylacetonate
L = Ligand

Table 6. General Reactions of ML_x^+ with $C_3H_7NH_2$

I. NH_3 Elimination

$$M(L)_x^+ + C_3H_7NH_2 \longrightarrow M(L)_x(C_3H_6)^+ + NH_3$$

II. Propene Elimination

$$M(L)_x^+ + C_3H_7NH_2 \longrightarrow M(L)_x(NH_3)^+ + C_3H_6$$
$$\longrightarrow M(L)_{x-1}(NH_3)^+ + C_3H_6 + L \text{ etc.}$$

III. Hydrogen Elimination

$$M(L)_x^+ + C_3H_7NH_2 \longrightarrow M(L)_x(C_3H_7N)^+ + H_2$$
$$M(L)_x(C_3H_7NH_2)^+ + C_3H_7NH_2 \longrightarrow M(L)_x(C_6H_{16}N_2)^+ + H_2$$

IV. Olefin and Carbene Elimination

$$M(L)_x^+ + C_3H_7NH_2 \longrightarrow M(L)_x(CH_3NH_2)^+ + C_2H_4$$
$$\longrightarrow M(L)_x(C_2H_5NH_2)^+ + CH_2$$

V. Adduct Formation

$$M(L)_x^+ + (C_3H_7NH_2) \longrightarrow M(L)_x(C_3H_7NH_2)^+$$
$$\longrightarrow M(L)_x(C_3H_7NH_2)^+$$

Table 7. Branching Ratios - % of Total Reaction

		Fe^+ (L = CO)	Ni^+ (L = CO)	Ni^+ (L = PF_3)
I	$M^+ + C_3H_7NH_2 \longrightarrow N(NH_3)^+ + C_3H_6$	16%	-	-
	$\longrightarrow M(C_3H_6)^+ + NH_3$	2%	-	-
	$ML + C_3H_7NH_2 \longrightarrow M(NH_3)^+ + C_3H_6 + L$	33	-	-
	$\longrightarrow M(C_3H_6)^+ + NH_3 + L$	15	-	-
	$\longrightarrow ML(NH_3)^+ + C_3H_6$	23	-	-
II	$M^+ + C_3H_7NH_2 \longrightarrow M(C_2H_5NH_2)^+ + CH_2$	3	-	-
	$ML^+ + C_3H_7NH_2 \longrightarrow M(C_2H_5NH_2)^+ + CH_2 + L$	-	26	-
III	$M^+ + C_3H_7NH_2 \longrightarrow M(C_2H_5N)^+ + CH_4$	5	100%	-
	$ML^+ + C_3H_7NH_2 \longrightarrow M(C_2H_5N) + CH_4 + L$	18	-	-
IV	$M^+ + C_3H_7NH_2 \longrightarrow N(CH_3NH_2)^+ + C_2H_4$	66	-	-
	$ML^+ + C_3H_7NH_2 \longrightarrow N(CH_3NH_2)^+ + C_2H_4 + L$	-	74	73
	$\longrightarrow ML(CH_3NH_2)^+ + C_2H_4$	-	-	27
V	$M^+ + C_3H_7NH_2 \longrightarrow M(C_3H_7N)^+ + H_2$	8	-	-
	$ML^+ + C_3H_7NH_2 \longrightarrow M(C_3H_7N)^+ + H_2 + L$	11	-	-

be expected containing the metal ion. Furthermore, Cu^+ and CuL^+ were not precursors to the product ions. This indicates that the products contain only the amine and amine fragements. These major ions were m/z of 89 and 119 and would be $(amine{\cdot}H{\cdot}CH_2NH_2)^+$ and $(Amine{\cdot}AmineH)^+$, respectively. Clustering has been reported previously with basic ligands and of basic ligands around M^+[54-56]. Metal assisted organic cluster formation, as with Cu^+ has not been reported.

C. Discussion

All of the metal ions except Fe^+ exhibited chemistry similar to that observed previously with alkanes. Copper and Chromium eliminate hydrogen, nickel selectively inserts into carbon-carbon bonds to eliminate methane and ethylene, manganese and zinc are totally unreactive other than formation of the adduct. Except for a certain preference for CH_4 elimination, iron was characteristically nonselective in its insertion. It inserted into C-H leading to H_2 elimination, C-N for NH_3 and C_3H_6 elimination, terminal C-C for CH_4 elimination, and the center C-C bond for CH_2 elimination. Using the literature M^+-CH_3 values as an estimate of M_+-C_3H_7 bond strenghts, an upper limit for the C_3H_7-M^+-NH_2 bond strength can be determined, assuming the $C_3H_7Fe^+$-NH_2 insertion intermediate is formed in an exothermic/thermoneutral process.

Refering back to analysis of the Co^+-NH_2 bond, lack of reactivity with amines is attributed to failure of M^+ to insert into the C-N bond in the first step of the mechanism. Since all steps of the mechanism are thermoneutral or exothermic this implies that

$$D°(M^+-NH_2) < D°(C-NH_2) - D°(M^+-C_3H_7)$$

for example the $C-NH_2$ bond strength is 80 ± 4 kcal/mole and $D°(Cr^+-CH_3)$ is 37 ± 4 kcal/mole so $D°(Cr^+-NH_2)$ is less than 43 kcal/mole. The limits on bond strengths are summarized below:

Table 8. Implied M^+-NH_2 Bond Strengths

Ion	Observation Insert into $C-NH_2$?	M^+-CH_3 kcal/mole	Implication M^+-NH_2 Bond Strength kcal/mole
Cr^+	no	37 ± 7	< 43
Mn^+	no	71 ± 7	< 9
Fe^+	yes	68 ± 4	> 12
Co^+	no	61 ± 4	< 19
Ni^+	no	48 ± 5	< 32
Cu^+	no	∿ 48	< 32
Zn^+	no	67 ± 1	< 13

The limits of first row transition metal-NH_2 bond strengths are unusually low, as was that of Co^+.

For explanation of this first examine Beauchamp's correlation of bond strengths to promotion energy to achieve a $3d^n4s^1$ configuration. Ground state configurations are listed below. As stated in the introduction, it is believed that Cr^+ from electron impact on $Cr(CO)_6$ and Mn^+/Mn_2^+ from $Mn_2(CO)_{10}$ may be populated in lower excited states. However for this analysis assume that only the ground state configurations are present:

$$Cr^+ - 4s^0\ 3d^5$$
$$Mn^+ - 4s^1\ 3d^5$$
$$Fe^+ - 4s^1\ 3d^6$$
$$Co^+ - 4s^0\ 3d^8$$
$$Ni^+ - 4s^0\ 3d^9$$
$$Cu^+ - 4s^0\ 3d^{10}$$
$$Zn^+ - 4s^1\ 3d^{10}$$

If a $4s^1$ electron is indeed necessary for bonding, a lack of reactivity of Cr^+, Co^+, Ni^+, and Cu^+ is readily explained. Energy is required in the course of the reaction to promote a 3d electron to the 4s orbital for bonding to occur, but this is only relevant to forming <u>one</u> bond not two. For example

$$Cr^+ \xrightarrow[\text{promotion energy}]{34.2\ \text{kcal/mole}} (Cr^+)^*$$

$4s^03d^5$ — non bonding form

$4s^13d^4$ — bonding form

The total energy for metal insertion must be written as

$$D^\circ(M^+\text{-}NH_2) \overset{?}{>} D^\circ(C\text{-}NH_2) - D^\circ(M^+C_3H_7) - \text{P.E. } 4s^13d^n \quad (11)$$

This analysis, however, does not explain the lack of reactivity of Mn^+ and Zn^+. What is unique to these ions is that they have stable filled and half-filled d oribitals. The significance of $4s^13d^5$ and $4s^13d^{10}$ becomes more clear if it is assumed that the insertion step required formation of <u>two</u> bonds. Since M^+-alkyl bonds require unpaired electrons, Mn^+ and Zn^+ are obviously in the wrong electronic configuration for insertion since they have only one unpaired electron.

Ab-initio calculations suggest that first row transition metal species MH_2 and MX_2 are linear with <u>sp hybrid orbitals</u>. By analogy, for insertion to occur the necessary promotion energy is not that to a $4s^13d^n$, but may be to a $4s^14p^13d^n$ or even a $4s^23d^n$ configuration. The total energy equation for metal insertion can be written:

$$\text{Total Energy} = \underset{\text{(Bond Breaking)}}{\text{Energy In}} - \underset{\text{(Bond Formation)}}{\text{Energy Back}} - \underset{\text{(Formation of } 4s^14p^13d^n\text{)}}{\text{Rearrangement Energy}} \quad (12)$$

The table below lists the ground state configuration of each of the metal ions, and whether it satisfies the requirements for bonding. Fe^+ is the only ion which could most readily form both the first and second bond in construction of the insertion intermediate because it has a 4s electron, and because the second electron is not associated with the extra stable filled or half-filled d orbital configuration. Fe^+ was the only ion which experimentally was found

Table 9. Electronic Configuration M^+ and Bonding

M^+	CONFIGURATION	4S 3D	FIRST BOND	SECOND BOND
Cr^+	$4s^0\ 3D^5$	↑ ↑ ↑ ↑ ↑	NO	---
Mn^+	$4s^1\ 3D^5$	↑ ↑ ↑ ↑ ↑ ↑	YES	NO
Fe^+	$4s^1\ 3D^6$	↑ ↑↓ ↑ ↑ ↑	YES	YES
Co^+	$4s^0\ 3D^8$	↑ ↑↓ ↑↓ ↑ ↑	NO	---
Ni^+	$4s^0\ 3D^9$	↑ ↑↓ ↑↓ ↑↓ ↑	NO	---
Cu^+	$4s^0\ 3D^{10}$	↑ ↑↓ ↑↓ ↑↓ ↑	NO	---
Zn^+	$4s^1\ 3D^{10}$	↑ ↑↓ ↑↓ ↑↓ ↑↓ ↑↓	YES	NO

to insert. This assumption is valid only if we also assume that, once in the appropriate M^{+*} configuration, all M^{+*}-bonds have the same strength for a given R.

Table 10 below lists promotion energies to achieve $4s^13d^n$, $4s^23d^n$ and $4s^14p^13d^n$ configurations. Since no $4s^14p^13d^n$ state has yet been observed for Cr^+ and Ni^+ actual promotion energies are not available. However, consideration of the energies required to promote a d electron to an s and a p orbital separately suggest that the promotion energies for these two ions are similar and that their promotion energies should fall between the values for Co^+ and Cu^+. This more quantitative analysis just repeats the information in Table 3. Here it has been shown that the only metal ion which inserts into the C-NH_2 bond is the ion with the lowest promotion energy to any of the proposed bonding configurations. These promotion energies cannot be used quantitatively to calculate the actual bond strength since the bonding configuration may not be purely $4s^14p^13d^n$ or $4s^23d^n$. They do indicate an ordering of energies involved in the rearrangement of electrons for the metal ion insertion rection. Both sets of promotion energies given in Table 10 suggest that P.E.($M^+ \longrightarrow M^{+*}$) follow the trend:

$$Fe^+ < Co^+ < Cr^+ \lesssim Ni^+ < Mn^+ < Zn^+ < Cu^+$$

If (NH_2-M^{+*}—C_3H_7) and ($C_3H_7M^{+*}$—NH_2) are each approximately independent of M, no ion with a PE > PE(Co^+) would be expected to insert into the C-N bond of propylamine; since it has been suggested that Co^+ does not insert into the C-N bond. The only possible candidate for insertion, then, would be the Fe^+ ion. The $Fe^+(C_3H_6)$ and $Fe^+(NH_3)$ products indicates that Fe^+ does insert into this bond.

Table 10. Promotion Energies of First Row Transition Metal Ions

M^+ Ground State Configuration	Cr^+ $3d^5$	Mn^+ $3d^5rs^1$	Fe^+ $3d^64s^1$	Co^+ $3d^8$	Ni^+ $3d^9$	Cu^+ $3d^{10}$	Zn^+ $3d^{10}4s^1$
$PE(s^1d^n)$[a]	34.2	0	0	9.6	24.0	62.7	0
$PE(s^1p^1d^n)$[b]	<380.4	238.0	155.8	229.6	<418.6	308.6	296.4
$PE(s^2d^n)$[c]	148.5	153.6	65.3	113.9	<418.6	195.2	175.6

a Promotion Energy (kcal/mole) required to reach the atomic ions lowest s^1d^n configuration

b Promotion Energy (kcal/mole) required to reach the atomic ions lowest $s^1p^1d^n$ configuration

c Promotion Energy (kcal/mole) required to reach the atomic ions lowest s^2d^n configuration

Further, the PE's correlate with the previously suggested metal reactivity trends. Ions with relatively high PE's are much more "selective" of the bonds into which insertion occurs (i.e., is exothermic), while ions with low PE's insert into many types of bonds.

The important point about the electronic configuration listed in Table 10 is not whether the two electrons are in an 4s or a 4p orbital, but that there are two unpaired electrons in orbitals other than the 3d orbital. It is these two electron which form the two bonds necessary for the metal insertion step.

The possibility of sp hybrids has been suggested in other systems. In 1957 Jorgensen noted the tendancy of d^{10} ions to form linear complexes[58]. This geometry also related to promotion energy to the $nd^9(n+1)s^1$ and $nd^9(n+1)p^1$ configurations. Au^+, Hg^{++}, and Cu^+ ions had the lowest excited states and the greatest tendancy to form linear complexes. Later Orgel modified this hypothesis suggesting that mixing d_z^2 orbital also is important. The relative importance of this term depends on the magnitude of d-s energy separation. The smaller the energy gap, the more extensive the d-s mixing[58]. Mingos has used symmetry arguments to conclude that the metal electronic configuration influences homolytic metal-carbon bond dissociation, a process similar to metal insertion[59]. Chatt and Shaw suggested that instability of transition metal alkyl and aryl derivatives is due to facile promotion of bonding d orbitals to antibonding sp sigma metal-carbon orbitals[60]. Stability of these organometallics is related to the energy separation of the two types of orbitals.

The significance of sp hybridization or bonding and of ground state configuration has been noted for several years by a number of groups in different studies. The importance of electronic configuration on the chemistry of gaseous metal ions was not intially obvious in the development of the insertion mechanism because M^+ insertion is typically a facile, exothermic process.

This is because the strengths of the bonds formed are usually much greater than the strength of the bond which is broken. Only in a system such as the amine where the bond strength is situated fortuitously between those of M^+-CH_3 and C-NH_2 does the effect become noticable.

CHAPTER V

EXTENDED HÜCKEL STUDIES OF METAL-AMINE INTERACTIONS

V. Extended Hückel Study of Nickel-Amine Interactions

A. Introduction

The chemistry of first row transition metal ions with propylamine provided an interesting correlation between reactivity and ground state configuration - the only ion which inserted into the C-N bond was Fe^+ which also had the lowest promotion energy to the $4s^1 4p^1 3d^n$ electronic configuration.

It is reasonable to assume that a doubly bonded metal ion would be sp hybridized since it has been shown for MH_2 and MX_2 species where X is a halide. In fact, general molecular orbital theory out of a descriptive inorganic textbook predicts such bonding[45]. Further, the tendancy of d^{10} ions to form linear complexes has been correlated with the energies of the Nd^9 (N+1)s and Nd^9(N+1)p excited states[58].

The question which remains is whether the product of metal ion insertion C_3H_7-M^+-NH_2, is also sp hybridized. Ab-inito calculations on such a large system would be very expensive. Instead, the question is addressed by Hückel molecular orbital theory. Hückel is the theory most widely used by experimentalists because it is relatively simple and can therefore be applied to a series of compounds and perhaps correlate properties. Note that the extended Hückel theory includes sigma as well as pi interactions.

Extended Hückel theory has been used extensively by Hoffmann and co-workers to evaluate trends in stereochemistries of transition metal complexes[61-69]: geometries of metals with ethylene and alkyl ligands[61,62], of M_2L_6 and M_2L_9 dimers[65-67], and of 16 electron cyclopentadiene compounds, to name just a few. Hoffmann has also used it in the study of reaction mechanisms to generate a reaction coordinate[63,68]. Anderson has studied chemistry of single crystal surfaces - chemisorption and surface

migration[70,71].

The purpose of this study is to determine the bonding characteristics of the metal insertion intermediate - is it primarily an sp hybrid and why is the bond so weak? Before answering those questions a comparison of extended Huckel, ab-initio, and MINDO calculations on nickel hydride and nickel dihydride is made in order to evaluate specific strengths and weaknesses.

B. Principles of Molecular Orbital Calculations

The first postulate of quantum mechanics is that all of the information describing a n-bodied system can be contained in a wavefunction- ϕ. The more precise the wave function, the more accurate the resulting properties such as ionization potential, bond length, or atomic charge[73].

The wave function can be thought of as an amplitude function which defines regions of different probability or density. The probability of finding an electron at a point in space is directly proportional to ϕ^2 at that point.

By mathematically defining regions of high electron density in a system, on a time averaged basis, physically meaningful information such as shapes of atomic orbitals or regions of high electron density in molecules (bonds) can be defined. The requirements on $\phi(x)$ are that it be single valued, finite, and continuous for all phyxcially possible values of x.

A most useful set of wave functions are those which describe atomic orbitals - ϕ_i.

Atomic orbitals contain primary types of information, the radial distribution R(r) and the angular component Y (σ,η) which describes shape in three dimensions:

$$\phi = R(r)\ Y(\sigma,\eta)$$

Consider for example the simple hydrogen 1s orbital:

$$\phi_{1s} = \left(\frac{1}{\pi a_o^3}\right)^{\frac{1}{2}} \exp\left(\frac{-r}{a_o}\right) \qquad (14)$$

where:

$$a_o = \frac{k_o \hbar^2}{Me^2} = 5.292 \times 10^{-11} \text{ meters (bohr)}$$

k_o = 4 pi x 8.854×10^{-12} farads/meter (permittivity of free space)

$\hbar$ = 1.055×10^{-34} joule second

m = 9.11×10^{-31} kg (electron mass)

e = 1.602×10^{-19} coulombs (proton charge)

r = distance in meters

By inspection, it can be seen that the hydrogen 1s orbital is spherically symmetric (no angular dependance) and falls off exponentially in the radial direction..

Properties can be calculated using operators. An operator is an accepted convention for transforming one function into another. An example is the momentum operator:

$$\hat{p}_q = -i\hbar(\partial/\partial q) \qquad (15)$$

q = coordinate

$\hbar = (\frac{1}{2\pi})$(Plank's Constant)

The most important operator is the Hamiltonian operator - $\hat{H}$, which operates on a wave function to produce system energy. It is composed of both kinetic and potential energies. The equation describing energy of a system is the Schroedinger equation, which for a one particle system has the form:

$$\hat{H}\phi = E\phi = \frac{-h^2}{2m} \nabla^2\phi + V\phi \qquad (16)$$

$\nabla^2 \equiv$ The Laplacian operator

$$= \frac{\partial^2}{\partial x^2} + \frac{\partial^2}{\partial y^2} + \frac{\partial^2}{\partial z^2} \qquad (17)$$

V = Potential energy operator

E ≡ Energy eigenvalue

For even relatively small systems the complete Hamiltonian retains an unwieldly number of terms. For example ethylene has sixteen electrons and six nuclei. The Hamiltonian has 18 nuclear kinetic energy terms, 48 electron kinetic energy terms, 96 electron - nucleus potential energy attraction terms, and 120 electron-electron potential energy repulsion terms.

The Hamiltonian operates on the wave function ϕ to produce system energy E without altering the wave function. E is a constant, and is called an eigenvalue. Energy values are discrete rather than continuous because the electron in ϕ is constrained to a finite space.

Calculation of the exact energy of a system requires exact $\hat{H}$ and ϕ. $\hat{H}$ can be precisely described, but in a many-bodied system ϕ must be approximated because it is very difficult to obtain a solution of (16). The various quantum mechanical techniques correspond to the types and level of these approximations. Commonly adjusted variables are described below.

A typical approach in constructing a molecular orbital is to assemble

it from atomic orbitals. This is called the Linear Combination of Atomic Orbitals - Molecular Orbital (LCAO-MO) technique. A general molecular orbital is:

$$\psi_j = \sum_r C_{jr}\phi_r \qquad (18)$$

ψ_j = j^{th} molecular orbital

ϕ_r = r^{th} atomic orbital

C_{jr} = r^{th} coefficient of j^{th} molecular orbital

The constraint for acceptable ψ_j is that the linear combination belongs to one of the irreducible representations of the point group of the molecule. This is because symmetry operations produce indistinguishable configurations (commutes with the Hamiltonian), and both the symmetry operators and the Hamiltonian share the same eigenfunctions. In a molecule, the symmetry of the total electronic ground state will be the product of the irreducible representations of occupied ψ_j.

Another approximation concerns correlation of electrons. For a many electron atom, or molecule the interelectronic repulsion terms in the potential energy portion of the Schroedinger equation make it impossible to solve exactly. A common approximation is to ignore the fact the electron motion is correlated. This is equivalent to ignoring the overall orchestration of electron movement by which they tend to avoid each other. Wave functions which ignore this property are constructed from a single determinant of one electron wave function.

Improvements on an initial ψ can be guided by the variation principle. According to this principle, first stated by Sir Rayleigh; better choices of ψ give lower values of E, and there is only one ψ which exactly defines a system. As an example, consider a simple two atomic orbital basis set for a molecular

orbital:

$$\psi = C_1\phi_1 + C_2\phi_2 \tag{19}$$

When applied to the Schroedinger equation (6), the result in short hand notation is:

$$E = \frac{C_1^2H_{11} + 2C_1C_2H_{12} + C_2^2H_{22}}{C_1^2S_{11} + 2C_1C_2S_{12} + C_2^2S_{22}} \tag{20}$$

$$H_{ii} = \int \phi_i H \phi_i \, \partial\tau \quad \text{(coulomb integrals)} \tag{21}$$

$$H_{ij} = \int \phi_i H \phi_j \, \partial\tau \quad \text{(resonance integrals)} \tag{22}$$

$$S_{ij} = \int \phi_i \phi_j \, \partial\tau \quad \text{(overlap integrals)} \tag{23}$$

To apply the variation principle, the partial derivatives of (20) with respect to C_1 and C_2 are set equal to zero. The result here is two linear equations in two unknowns. Matrix mathematics can be applied to give a 2 x 2 secular determinant:

$$\begin{vmatrix} H_{11}-ES_{11} & H_{12}-ES_{12} \\ H_{11}-ES_{21} & H_{22}-ES_{22} \end{vmatrix} = 0 \tag{24}$$

Values of E which satisfy the equation are the energies of the system; in this case two energies correspond to energies of two molecular orbitals. In general, the size of the determinant equals the number of atomic orbitals in the basis set, and therefore the number of energies and molecular orbitals.

Determination of energies requires values for the three types of integrals. S_{ij} can be solved exactly if geometry of the molecule is known. The

approximate methods for determining H_{ii} and H_{ij} can be categorized as to whether or not they are iterative. These that are iterative, adjust and readjust to a point of self consistancy in the energy eigenvalue - E. These are called Self Consistent Field (SCF) calculations. The noniterative calculations give little energetic information, but provide semi-quantitative orbital mixing and insights into geometry. It is this second type of technique, specifically the extended Hückel molecular orbital method, which is used for the theoretical aspects of this thesis.

Ab-initio calculations have the fewest approximations. All terms are included in the Hamiltonian.

Of the iterative calculations there are two catagories. Both techniques retain the SCF methodology, some parameterize the various integrals ("NDO" techniques - neglect of differential overlap) and some do not. The "NDO" methods are fast and have been successful in reproducing spectroscopic and geometric properties of organic molecules, but have not been developed as extensively for metal systems[74].

C. The Extended Hückel Method

In the extended Hückel molecular orbital method, both pi and sigma interactions are included. The basis set of atomic orbitals are usually Slater Type Orbitals-ϕ i. The STO radial function is given by:

$$R(r) = r^{(n^*-1)} e^{(-\zeta r)} \qquad (25)$$

where

$$\zeta = \frac{Z_e}{n} \qquad (26)$$

Z_e = effective nuclear charge

n = principal quantum number

The size of the radial function is adjusted by varying Ze - increasing Ze makes the atomic orbital "shrink" closer to the nucleus. The STO's are good representations of the radial functions, especially when close to the nucleus. In this thesis, Gaussian expansions of STO's are used. These functions are considered to be accurate representations of the Slater orbitals. Figure 3 describes STO's for first row transition metals.

The S_{ij} values in (24) are evaluated using (25). S_{ii} are set equal to one, which normalizes the molecular orbitals.

The values of H_{ii} are typically set equal to valance orbital ionization potential (VOIP). This, of course, changes with the charge on the atom, and with its configuration. Typically, small differences in VOIP do not affect the qualitative aspects of the results.

The off-diagonal elements in the determinant (24) are estimated with the Wolfsberg-Helmholtz approximation:

$$H_{ij} = (\tfrac{1}{2})(K)(S_{ij})(H_{ii} + H_{ij}) \qquad (27)$$

$$K = \text{a constant}$$

The greater the overlap between orbitals, S_{ij}, the greater this contribution is to total system energy. A special case is the treatment of pi bonding only, where S_{ij} is often arbitraily set to zero, and therefore $H_{ij} = 0$. These simple calculations have produced a good correlation with experimental "resonance energies" of extended pi systems.

Once the integrals are evalulated and roots of the determinant established; values of C_j are placed into equation (18) for the resulting molecular orbital. Knowledge of ψ_j permits the following evaluations:

Figure 3: Radial Expectation Values in a_0

	$(r)_{3d}$[a]			$(r)_{4s}$[b]
Atom	$4s^2 3d^{n-2}$	$4s 3d^{n-1}$	$3d^n$	$4s^2 3d^{n-2}$
Sc	1.675	2.069	2.641	3.98
Ti	1.460	1.725	2.098	3.80
V	1.323	1.522	1.775	3.65
Cr	1.219	1.368	1.610	3.52
Mn	1.130	1.275	1.468	3.40
Fe	1.073	1.189	1.352	3.29
Co	1.016	1.114	1.254	3.18
Ni	0.965	1.050	1.169	3.09
Cu	0.918	0.991	.	3.00

[a]From P. J. Hay, J. Chem. Phys. 66, 4377 (1977).

[b]Calculated using wavefunctions give by A. J. H. Wachters, J. Chem. Phys. 52, 1033, (1970).

1. The net atomic population is the fraction of total electron density in a molecular orbital which can be assigned to atom i. The quanitity is $n_i(C_i)^2$ where n = number of electrons in the molecular orbital.
2. The atomic overlap population, $2(C_i)(C_j)(S_{ij})(n)$ is a measure of the number of electrons shared between two atomic orbitals ϕ_i and ϕ_j. If this value is summed for <u>all</u> k orbitals on atom x with <u>all</u> k orbitals on atom y, the atom-atom overlap results:

$$\text{Atom-Atom Overlap Population} = \sum_{k} (2)(n)(C_i)(C_j)(S_{ij}) \qquad (28)$$

This atom/atom overlap population is related to bond strength for bonds of similar ionic character.

3. The gross atomic population analysis assigns all of the electron density in a molecule to the individual atoms. The electron density between atoms is split equally, rather than being weighted according to electronegativity.

$$\text{Gross Atomic Population} = \sum_{\substack{\text{all} \\ \text{m.o.}}} [(n)(C_i^2) + (n)(C_1)(C_2)(S_{ij})] \qquad (29)$$

4. The formal charge is the core charge less the gross atomic population. Core charge is the sum of the nucleus plus non-valence electrons.
5. Electron density between atoms indicates the build up of electrons between atoms, and is the best measure of bond order.

Usefullness of EHMO Results

The EHMO theory has been effective in predicting geometry, and barrier to rotation. For example, the energy between staggered and eclipsed ethane

is calculated to be 4.0 kcal/mole. The experimental value is 2.7 to 3.0 kcal/mole[75]. Good evaluations of angular geometry are the result of exactly evaluating the overlap integral. Distance variation of the overlap integral and of total energy are crude because the nuclear-nuclear repulsions are not included in the Hückel Hamiltonian. As an example, the lowest energy of H_2 molecule is at $S_{ij} = 1$ which occurs when bond length is zero! Predictions of electronic and photoelectron spectra are also dependent on the quality of wave function used and so are usually inadequate. Similarly, thermodynamic information is expected to be semiquantitative at best.

A major short coming of EHMO theory is it's inability to deal with states of multiplicity higher than a doublet. Once the coefficients of atomic orbitals have been set, and the molecular orbital energies determined, the lowest energy will always be that of lowest multiplicty. This is because total energy is simply the sum of the energies of occupied molecular orbitals. Therefore putting an electron into a higher molecular orbital will always increase the total energy. No further adjustments and readjustments on the new total M.O. are included to offset this change. Iterative (SCF, ab-initio) calculations would be able to compensate this energy loss. Therefore EHMO theory will never predict the ground state of a molecule to have more than one unpaired electron. Rather, the true multiplicity of a system should be known and used to guide interpretation of EHMO data.

D. Additional Nuclear-Nuclear Repulstion Term

As previously described, a short coming of EHMO theory is the lack of nuclear-nuclear repulsion terms in the Hamiltonian. The resulting calculated bond lengths frequently do not agree with experimental values.

Addition of a two-bodied repulsive term to the extended Hückel Hamiltonian has been shown to be yield good predictions of bond lengths and force constants[76,77]. This repulsion term is the integral of the Hellman-Feynman electrostatic force:

$$E_{total} = E_{Huckel} + E_{Repulsion} \tag{30}$$

$$E_{rep} = \sum_{\alpha<\beta}^{N} E_{\alpha\beta} \tag{31}$$

$$E_{rep} = \sum_{\alpha<\beta}^{N} -Z_\beta \int \rho_\alpha(r)(R_\beta - r)^{-1}\, d\tau \tag{32}$$

$Z_\beta \equiv$ Charge of nucleus of atom β

$\rho(r) \equiv$ ρ electronic (r) + $\Sigma\rho$ nuclear (r)

$\equiv$ atom α's electronic plus nuclear charge densities

$(R_\beta - r) \equiv$ distance atom β to point r

$N \equiv$ number of atoms in molecule

The system (illustrated in Figure 4) is described with the electronegativity of atom α greater than or equal to that of atom β. The <u>electron</u> contribution to the charge density used in (32) is that of the more electronegative atom.

$$\rho_{\alpha_{electronic}}(r) = \sum_{i=1}^{N_\alpha} \phi_{i\alpha} N_{i_\alpha} \tag{33}$$

For a carbon atom interacting with a hydrogen atom, would be the carbon atom, and charge density would be summed over both 2s and 2p (Slater type) orbitals:

$$\rho_{carbon}(r) = (\phi_{1s}^2)(2) + (\phi_{2p_x}^2)(nx) + (\phi_{2p_y}^2)(ny) + (\phi_{2p_z}^2)(nz) \tag{34}$$

$$2 = n_x + n_y + n_z \tag{35}$$

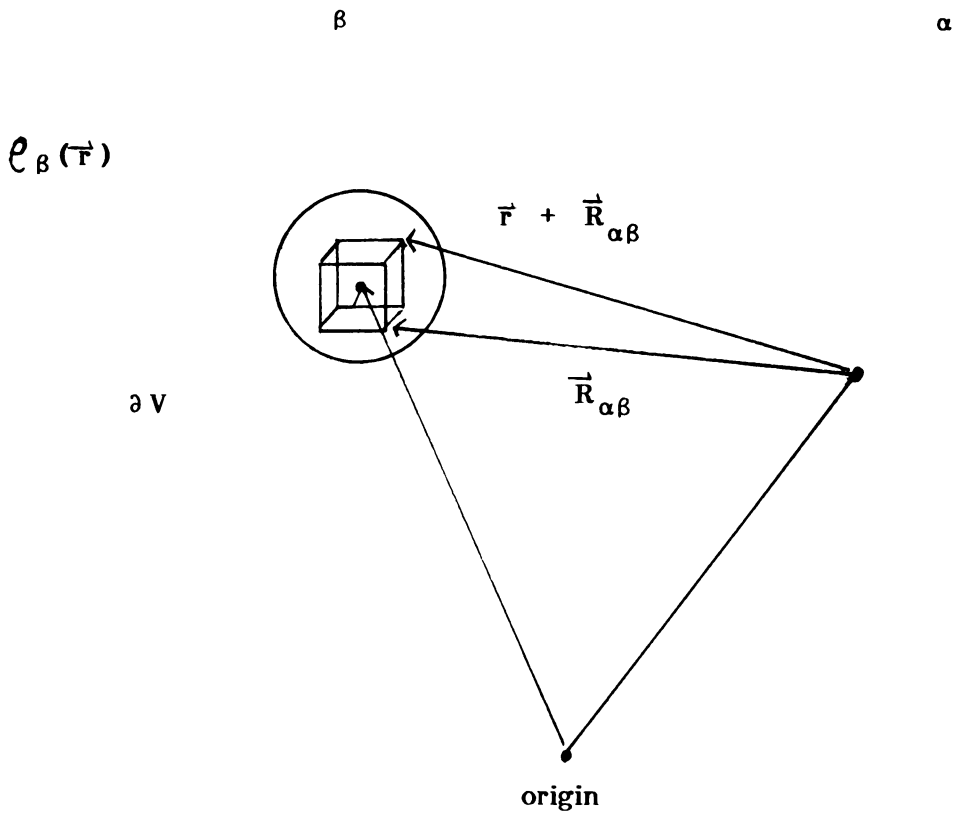

$$E(R) = \sum_{\alpha < \beta} E_{\alpha\beta}$$

Figure 4. Hellman–Freynman, Electrostatic Force Model

The repulsion term is a constant added onto the energy calcualted with EHMO treatment (equation 30), and therefore does not change the Hamiltonian or the resulting molecular orbitals ψ_i Examples of utility of this additional term are listed below:

Bond	Calculated	Experimental	Reference
C-H of formaldehyde	1.205 Å	1.102 Å	76
C-O of formaldehyde	1.184 Å	1.210 Å	76
Cu-Cu of Cu_2	2.26 Å	2.22 Å	77

CHAPTER VI

COMPARISON OF Ab-INITIO, SCF AND EHMO TREATMENTS OF NiH AND NiH_2

VI. Comparison of Ab-Initio, SCF, and EHMO Treatments of NiH and NiH_2

A. Nickel Hydride

Table 11 summarizes data for Nickel hydride. The ground state of the nickel atom is $4s^1 3d^9$, so both doublet and quartet states are possible for the hydride.

Ab-initio calculations give about two-thirds of the experimental dissociation energy, and the correct bond length of 1.47 $\mathring{A}$ [76].

Given below are representations of the axis system for both NiH and NiH_2:

NiH: 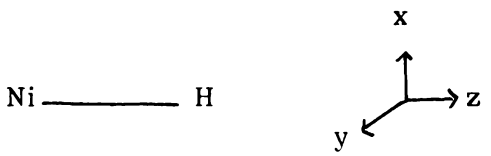

NiH_2: 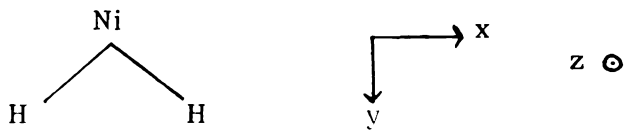

Calculations with a semiempirical SCF method were the most extensive[80]. The ground state configuration is $^2\Delta$. The bond length and dissociation energy exactly matched the experimental values because the system is parameterized with variables chosen exactly for this match. In agreement with all but one ab-initio calculation, bonding is found to be due to nickel s and p orbitals with the hydrogen 1s. Some contribution to the bonding molecular orbital occurs with Nid_z2, but it has negligible overlap with the hydrogen orbital. Finally, the noninteracting nickel d orbitals are lower in energy in NiH than in the atom and also lower than the sp hybrids. This is attributed to reduction of electron-electron repulsion as electron

Table 11. Analysis of NiH by Several Techniques

Technique	Bond Length Å	Multiplicity	Atomic Charge		Ni Hybridization			Bond Energy kcal/mole
			Ni	H	4s	4p	3d	
Experimental[78]	1.47	Doublet	-	-	-	-	-	70.8
Ab-Initio	1.47	Doublet	-	-	-	-	-	∿47
MINDO/SR	1.47	Doublet	+0.32	-0.32	.43	.43	8.79	70.8
Extended Huckel Energy #1								
$4s^1 3d^9$	1.30	Doublet	0.13	-0.13	0.69	0.10	9.1	285.7*
	1.47	Quartet	0.13	-0.13	0.69	0.10	9.1	285.7
$4s^2 3d^8$	1.30	Doublet	0.13	-0.13	0.69	0.10	9.1	353.7
$4s^1 4p^1 3d^8$	1.30	Doublet	0.13	-0.13	0.69	0.10	9.1	473.4
Energy #2								
$4s^1 3d^9$	1.30	Doublet	0.20	-0.20	0.64	0.05	9.1	182.9

* Energy = ΣNi atomic orbitals + **H1s orbital** - Σ NiH molecular orbitals

Energy 1: 4s = -10.7 eV 4p = -6.30 eV 3d = -13.2 eV (1979 values)

Energy 2: 4s = -8.66 eV 4p = -4.90 eV 3d = -12.99eV (1974 values)

density is shifted onto hydrogen. The charge on the hydrogen is -0.32.

EHMO Treatment of NiH

The first step is to test the sensitivity to the various input parameters. The criteria will be whether a change in a variable effects nickel hybridization at the equilibrium bond length. With the Anderson repulsion term added to the total energy, bond lengths can be calculated with reasonable accuracy. Since resulting molecular orbitals will depend on overlap of atomic orbitals they will also depend on bond length. Therefore it is important to use the bond length predicted by the extended Huckel program with the Anderson repulsion term and STO's.

Nickel has 9 electrons, and so there is a choice of 5 possible holes. For the $^2\Delta$ configuration, one of the d orbitals of quantum number 2 would have to be singly occupied. With the axis system oriented so that the NiH bond lies along the z axis, the d orbital assignments are as follows:

Orbital	Quantum Number*	Type Bond
d_{xy}	2	delta
$d_{x^2-y^2}$	2	delta
d_{yz}	1	pi
d_{xz}	1	pi
d_{z^2}	0	sigma

The equilibrium bond length for all electronic states is 1.30 Å. Figure 5 shows that for $4s^13d^9$, $4s^23d^8$ and $4s^13d^9$, the bond length is always 1.30 Å.

* The quantum number equals the number of nodal planes intersecting the z axis.

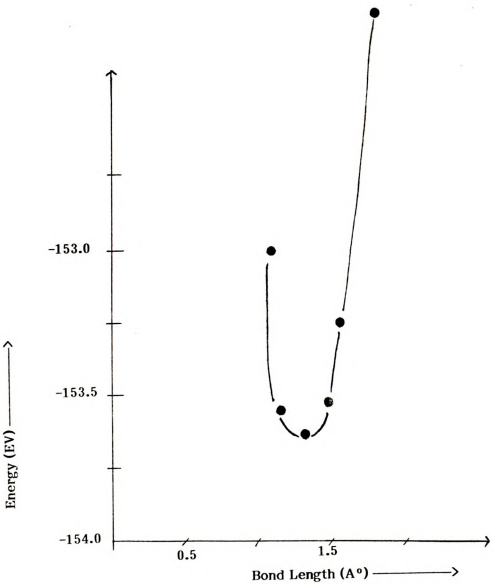

Figure 5 Ni-H Bond Length,Energy Set 1

Indications of nickel hybridization are given by atomic orbital occupancy. The numbers which will be used for the "hybridization" of an atom are estimated as the number of electrons in each of the particular atomic orbitals. They, individually, are calculated by summing contributions from two interactions: 1) electrons on the orbital which are shared with electrons of another orbital (bonding interactions), and 2) electrons which reside only with the atomic orbital (nonbonding interactions). For example, a doubly occupied nonbonding $3d_{xy}$ orbital would have a hybridization of two since two electrons reside solely within it and are not shared via bonding. This hybrization term is not affected by configuration: it is $4s^{.69}4p^{.09}3d^{9.1}$ for all three cases. This is to be expected for "hydridization" since electronic configuration is treated only in the Andersen repulsion term and does not affect calculation of the coefficients of the atomic orbitals in the molecular orbital. The change in the total energy simply represents the difference in initial orbital occupations. For example, the energy change from $4s^13d^9$ to $4s^23d^8$ is exactly the energy difference between an s and d orbital.

Several H_{ii} or valence orbital ionization potentials are available in the literature, having been developed by Hoffmann and co-workers in the past ten years. The two energy sets used in these calculations are given below:

Ni H_{ii} Parameters (EV)

	Energy Set #1 (1979 values)	Energy Set 2 (1974 values)
4s	-10.7	- 8.66
4p	- 6.30	- 4.90
3d	-13.2	-12.99

Figure 6 is the determination of bond length for another set of nickel H_{ii}. The increase in positive charge on the nickel is due to the greater energy separation between Ni 4s and H 1s, which causes a greater portion of electron density to go to the now relatively lower in energy H 1s. This is true because only bonding and nonbonding molecular orbitals are occupied. The difference is also due to the simple procedure by which bonding electron density is evenly distributed between two nuclei. Such a procedure will give most meaningful results when atom electronegativities are nearly equivalent. In the nickel hydride case, the more electronegative hydrogen atom is given a smaller portion of bonding density than it has in reality. In general, the assigned negative charge will always be less than it would in other calculations. The severity of this shortcoming would increase as the difference in electronegativities of bonding atoms increases. This effect is also tempered by the fact that, to a certain extent, electronegativity is included implicity in the calculation via the H_{ii}. However, the "in-situ" eletronegativity is not included. Similarly there is a small change in nickel "hybridization" with the second set of energies. The increase in the s,p energy gap results in a change of sp hybridization because atomic orbital mixing is a function of overlap - which decreases with increasing energy gap.

Multiplicity greatly affects bond length; the experimentally incorrect quartet state gives the experimentally correct 1.45 $\mathring{A}$ bond length, Figure 7. The sensitivity to multiplicity occurs because the Lowest Unoccupied Molecular Orbital (LUMO) of the doublet is being stabilized with increasing bond length more than the Highest Occupied Molcular Orbital (HOMO) - Figure 8. The interpretation of this relates to the atomic orbital mixing

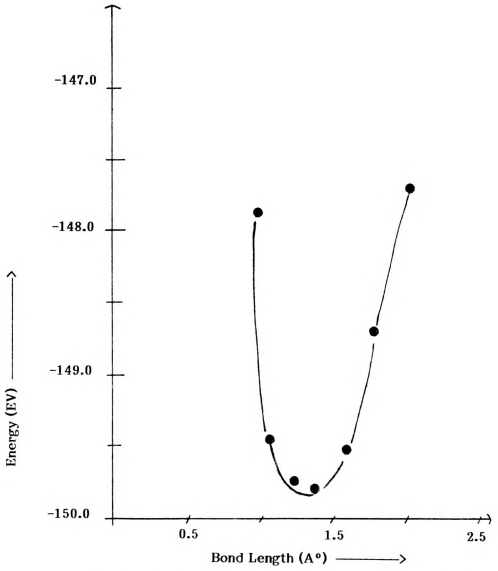

Figure 6 Ni-H Bond Length; Doublet State, Energy Set #2
Equilibrium Bond Length of 1.30 A°

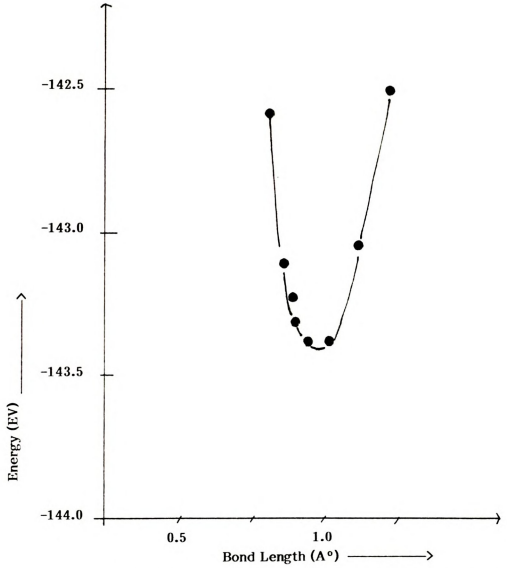

Figure 7 Ni-H Bond Length; Quartet State Energy Set #2
Equilibrium Bond Length of 1.50 A°

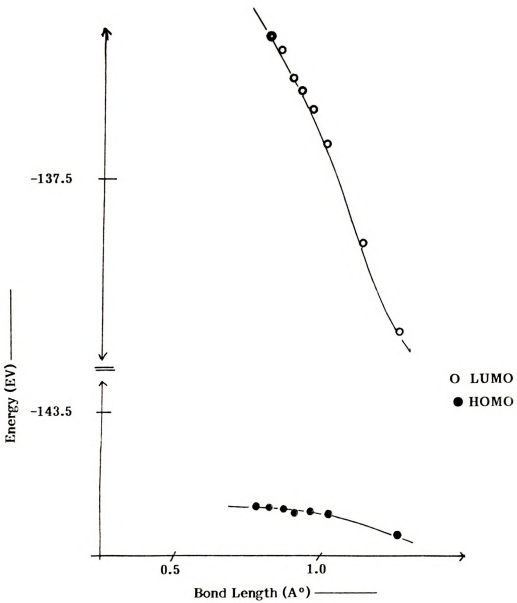

Figure 8. NiH: HOMO and LUMO Energy vs. Bond Length

in HOMO and LUMO. The LUMO contains significantly more 4s and 4p character. The 4s and 4p orbitals extend further radially than do the 3d. Therefore a given amount of bonding or overlap can be achieved at a larger separation of nuclei, with resultant decrease in repulsion terms. In fact, even without the addition of the E_{rep} term, the bond length increases with increase in multiplicity. The LUMO is an antibonding orbital. Increasing electron density in an antibonding orbital decreases overall bond order and would be expected to increase bond length.

The extended Hückel molecular orbital diagram, Figure 9, shows 4 nonbonding nickel d orbitals at their original energies; $d_{x^2-y^2}$, d_{xy}, d_{xz} and d_{yz} The singly occupied HOMO contains the $4d_{z^2}$ orbital. Therefore, the hole is in an orbital of quantum number zero-producing a $^2\Sigma$ state. This orbital is responsible for bonding to hydrogen:

$$HOMO = +(0.882)(d_{z^2}) - (0.434)(4s) - (0.01)(4p_x) - (0.12)(H1s)$$

There is considerable d_{z^2} character to this HOMO, primarily to orthogonalize the orbital. The actual, somewhat negligible, contribution of the d_{z^2} orbital to bonding is reflected in the atomic orbital overlap:

Overlap in Nickel Atomic Orbital Basis Set with Hydrogen 1s

Nickel Atomic Orbital	Overlap at 1.30 Å	Overlap at 1.45 Å
4s	0.47	0.40
$4p_x$	0	0
$4p_y$	0	0
$4p_z$	0.47	0.49
$3d_{x^2y^2}$	0	0
$3d_{z^2}$	0.23	0.20
$3d_{xy}$	0	0
$3d_{xz}$	0	0
$3d_{yz}$	0	0

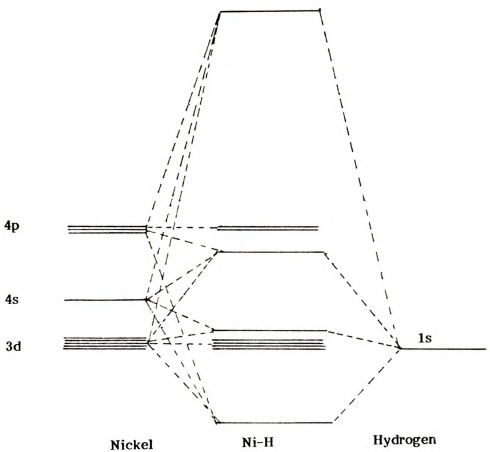

Figure 9. Extended Hückel Molecular Orbital Diagram of NiH

The considerable overlap of the 4s and 4p is explained by their greater radial extension in comparison to the 3d (refer to introduction section). Orbitals which have zero overlap are either symmetry forbidden to mix, or their energy gap is very significant.

Unlike the SCF calcualtions, nonbonding nickel d orbitals remained at their original energies. The reason for this difference is that EHMO is not an iterative procedure, so the d levels do not get an opportunity to adjust.

As expected, EHMO theory does not give meaningful quantitative thermodynamic results. However, it does give insight into nickel "hybridization" via atomic orbital occupancies. For both MINDO/SR and Hückel calculations, the total sp hybridization is 0.80. The weighting of s character, however, is greater for MINDO. Extent of p interaction in the Hückel program is supported by it's significant atomic orbital overlap values with hydrogen 1s. Differences in sp distribution are in part due to the different atomic orbital functions.

For the remaining calculations, the nickel electronic ground state configuration of $4s^1 3d^9$, and the 1979 energy set #1 values will always be used. Lowest multiplicity will always be ground state configuration, but higher multiplicities will also be examined. The typical electron-electron interactions which would compensate for higher multiplicities are on the order of 1.5 ev. Therefore if the extended Hückel HOMO-LUMO gap of a molecule is near this energy, higher multiplicity configurations should be considered to be viable possibilities.

B. EHMO Treatment of NiH_2

The first step of the EHMO treatment is to check the bond lengths for NiH_2. This was done by setting one bond at 1.30 Å as determined in NiH calculations, and then varying the second bond length with a $4s^1 3d^9$

nickel configuration. The result was a second bond length of 1.45 Å for both singlet and triplet states - figure 10 (Possible multiplicies are singlet, triplet, and quintet). It was next determined that the most stable configuration is with both bonds at 1.45 Å, so this value was used for further calculations.

Figure 11 is the variation of energy with H-Ni-H bond angle. The equilibrium geometry is 90° for the singlet and about 150° for the experimentally correct triplet state.

Several transition metal dihydrides have been treated at ab-initio and lower levels. Table 12 summarizes results of NiH_2.

There is good agreement across the board between experimental and calculated bond lengths. For extended Hückel this can be attributed to the additional nuclear/nuclear repulsion term.

There are two important Hückel configurations for NiH_2; singlet ground state with a 90° angle and the excited triplet state with a 150° angle. Comparison of results with ab-initio and MINDO/SR calculations is favorable. Geometry and atom charge match closely for the experimentally correct lowest energy triplet configuration. The "hybridizations" also match very closely; 1.71 sp hybridization for Mindo and 1.45 sp hybridization for Hückel. Both calculations also show an increase in sp and decrease in d orbital bonding for NiH_2 vs. NiH. The Hückel ground state singlet has the same trends, but to a lesser extent for the absolute amount of sp hybridization, and also the relative increase with addtion of another hydrogen to NiH.

The opening of the bond angle on increasing multiplicity can be explained by the molecular orbitals. The LUMO of the singlet state is antibonding with respect to hydrogen-hydrogen interactions. This is the orbital which becomes singly occupied in the triplet state, reducing interactions or bonding

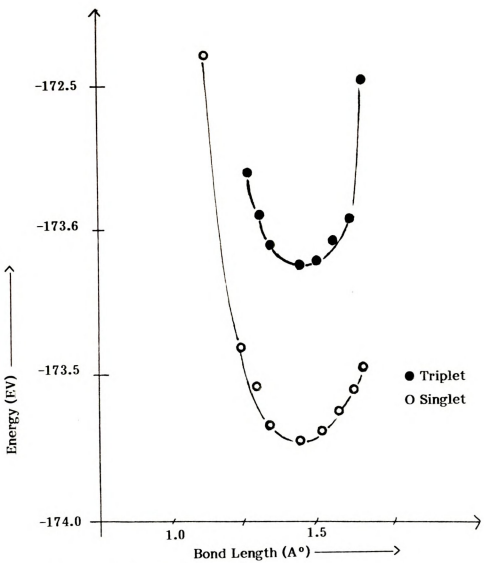

Figure 10 Linear NiH_2
Second Ni-H bond length vs. energy first Ni-H Bond Length 1.30 A°, singlet and triplet states

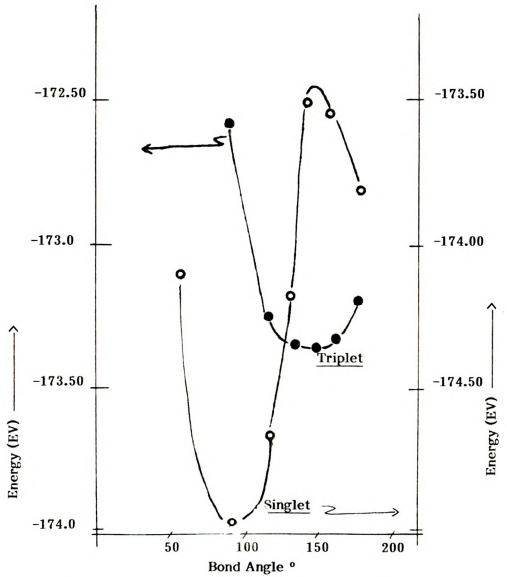

Figure 11. H-Ni-H Energy vs. Bond Angle for Doublet and Triplet States

Table 12. Summary NiH_2 Results

Technique	Bond Length Å	Bond Angle °	Multiplicity	Atomic Charge Ni	Atomic Charge H	Hybridization 4s	Hybridization 4p	Hybridization 3d
Experimental	1.45	180°	Triplet	-	-	-	-	-
MINDO/SR	1.47	175°	Triplet*	+0.31	-0.155	0.99	0.68	8.01
	1.46	90°	Singlet**	+0.24	-0.12	-	-	-
Ab-Initio	1.40	180°	Triplet	-	-	-	-	-
Extended Huckel	1.45	90°	Singlet*	+0.16	-0.08	0.69	0.25	8.74
	1.45	150°	Triplet**	+0.34	-0.17	0.95	0.51	8.13

* Ground State
** Excited State

density between hydrogens and therefore opening the angle.

$$\psi_{\text{LUMO}} = (-.82)(d_{xy}) + (.39)(4P_x) + (0.29)(H_a1s) - (0.29)(H_b1s)$$

singlet, 90°

A variable which is very sensitive to bond angle is charge on nickel and hydrogen:

Bond Angle	Charge on Hydrogen
25	+ 0.151
60	+ 0.026
90	- 0.080
135	- 0.137
150	- 0.172
160	-0.245
180	-0.245

As the bond angle decreases from 180°, charge leaves the hydrogen and moves onto the nickel atom. This reflects the fact that some of the electron density moves effectively to the rear of the molecule with decreasing angle. When this density is "behind" the nickel, it is not accessible to hydrogen, and therefore the charge on hydrogen becomes more positive.

At 180°, the EHMO hydrogen charge is more negative than with MINDO calculations. The opposite was true for NiH. The relative differences can be attributed to relatively higher Ni-H bond density (as indicated by the electron distribution between atoms) for NiH_2 than NiH in EHMO theory (0.37 vs. 0.33). Higher bonding density means more charge to distribute between atoms and therefore greater charge separation.

As with NiH, the non bonding d orbitals of NiH_2 remained at their original energy. In MINDO and ab-initio calculations the 4 nonbonding d orbitals lowered in energy, even below their level in NiH. This is attributed to even further reduction of d-d repulsions in NiH_2 compared to NiH.

The bent metastable states of singlet and quintet NiH_2 were thoroughly explored with MINDO/SR[80]. These species are pertinent to the mechanism of dissociation of H_2 over a nickel atom.

C. First Row Transition Metal Dihydrides

Calculations for other first row transition metal dihydrides are similar to NiH_2. In general they show a tendancy towards high multiplicity and towards bonding by two electrons outside the d shell. At the MINDO level, the $3d^n$ configuration of the metal does not significantly change to accomodate bonding which is primarily through the 4s orbital[81]. What metal 3d-hydrogen 1s interaction does occur is due to charge transfer via the metal 4s orbital.

The metal 3d-hydrogen 1s interaction, via metal 4s, changes across the 1st transition row. Lighter metals such as scandium and titanium have relatively strong interactions. For heavier first row transition elements the 3d orbital energy drops, and the radial extension decreases rapidly. Hence, metals such as nickel have weak 3d-1s interactions. One manifestation of this is the resistance to bending. Later first row transtion metals have less significant 3d mixing more sp hybridization, and more resistance to bending. For example, bending from 180° to 150° requires 14 kcal/mole for NiH_2 and less than 1 kcal/mole for TiH_2[80].

Ab-initio effective core potential calculations provide another point of view[82,83]. In these, d orbital participation is via back bonding from the

hydrogen 1s. Back bonding is a function of bond length and occupancy of d orbitals, but does not require p orbital participation. This was demonstrated by, again, resistance to bending. Metals with empty d orbitals: ScH_2 and VH_2, bend; but CrH_2 and ZnH_2 with half filled and filled d orbitals are linear. These effects were also observed when 4p orbitals were removed from the molecular orbital basis set.

D. Summarized Critique of EHMO Theory

The shortcomings of EHMO theory are: 1) it neglects electron correlation, and charge redistribution, 2) it does not always predict exact geometry, 3) in itself, it is incapable of predicting high multiplicity ground states - although examination of the molecular orbital's HOMO-LUMO gap provide some indication of the likelihood of higher spin states, and 4) it cannot quantify thermodynamic values.

Yet, these deficiencies are somewhat compensated by generation of molecular orbitals possessing the same general characteristics as those of ab-initio calculations The heart of the argument concerning first row transition metal hydrides and dihydrides was reproduced. The metal sp orbitals hybridize, and the extent of hybridization is greater with MH_2 than MH. The importance of the Anderson repulsion term is that it chooses the proper bond length which is critical for proper molecular orbitals and atomic orbital overlap.

Therein lies the value of EHMO theory. As a parameterized calculation it provides a simple means to correlate known physical properties with experimental results. EHMO results, then, are a foundation from which a rationalization process begins. The inexpense, and simplicity of the technique make it suitable for the study of many compounds which are not amenable to higher level calculations due to their size.

It was therefore decided to be worthwhile to extend the EHMO analysis of nickel compounds to the proposed intermediate of the metal ion-amine reaction.

CHAPTER VII

EHMO TREATMENT OF METAL ION INSERTION INTERMEDIATE

VII. EHMO Treatment of Metal Ion Insertion Intermediate

Analysis of the intermediate for metal ion insertion into the carbon-nitrogen bond of a primary amine will be via the fragment formalism. Each portion of the intermediate is constructed individually, and then the fragments are assembled. Given below are the coordinate systems for the fragments.

NH_2:

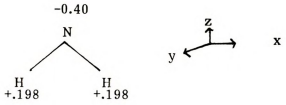

Ni-NH_2:

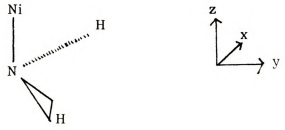

A. NH_2

The first choice in constructing NH_2 is of H_{ii} values for nitrogen and hydrogen. It has been shown that the calculated geometry of main group compounds depends on relative values of the atomic orbitals, or the np-ns separation[12]. For NH_2, the equilibrium bond angle determined by EHMO theory, is a function of 2s-2p hybridization. The extent of this hybridization is dependent on the energy separation. The H_{ii} values optimized for NH_3 geometry should also be the best choice for NH_2. Therefore H_{ii} values would be 2s at -28.0 eV, 2p at -9.0 eV, and hydrogen 1s at -15.0 eV. However, these

values and the 2s/2p energy separation differ from the H_{ii} developed for organometallics by R. Hoffman: 2s at -26.0 eV, 2p at -13.4 eV, and hydrogen 1s at -13.6 eV. For consistency, the entire R. Hoffmann basis set is used rather than independently optimized H_{ii}'s. This smaller than optimized 2s/2p gap would be expected to increase sp mixing and open up the equlibrium bond angle.

NH_2 has a single unpaired electron and will be a doublet. Calculations were done with the experimentally correct 1.02 Å bond length and 103.39° bond angle[13]. The resulting molecular orbitals are:

-30 Ev $1b_1(1) = (.69)(N_{2s}) + (.26)(H_{a1s}) + (.26)(H_{b1s})$

-18 Ev $1b_2(2) = (.65)(N_{p_x}) + (.38)(H_{a1s}) - (.38)(H_{b1s})$

-19.5 Ev $1a_1(3) = (.29)(N_{2s}) + (.91)(N_{p_y}) - (.12)(H_{a,b1s})$

-13.4 Ev $1(4) = (1.0)(N_{p_z})$

+11.25 Ev $(5) = (0.99)(N_{p_x}) - (.86)(H_{a1s}) + (.86)(H_{b1s})$

+32.67 Ev $(6) = (-1.09)(N_{2s}) + (.65)(N_{p_y}) + (.87)(H_{a1s}) + (.87)(H_{b1s})$

The unpaired electron goes into the 4th molecular orbital which is a pure Pz orbital, perpendicular to the plane of the molecule. The EHMO ground state configuration then, is $^2B_1$. Charge has transferred onto the nitrogen leaving the hydrogens at +0.198.

Ni-NH_2

First the bond length is determined using planer geometry. The 1979 H_{ii} values from the NiH_2 calculations, and $4s^13d^9$ configurations were used. Combination of doublet NH_2 and triplet nickel can produce doublet and quartet states. Figure (12) shows that the bond length for the doublet state is 1.85 Å - within ± 0.05 Å. This compares favorably with the experimental

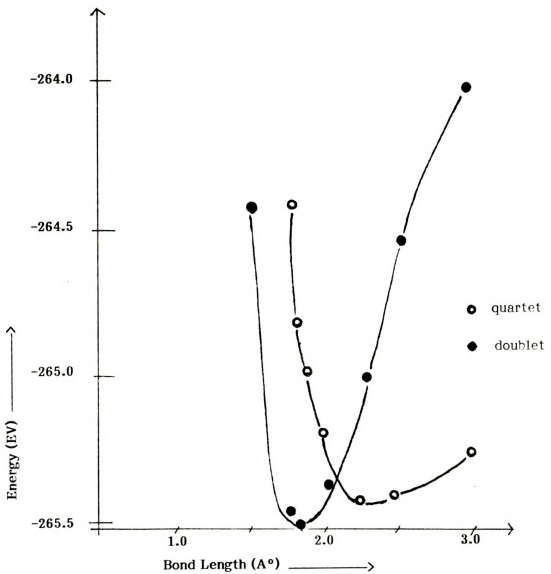

Figure 12. $NiNH_2$, Energy vs. Ni-NH_2 Bond Length
Nickel $4s^1\ 3d^9$ Ground State

$Ni-NH_3$ length of 1.87 Å [88]. The quartet state's bond length is greater than the doublets - 3.25 Å. The explanation of this is similar to that with NiH. The doublet state LUMO contains anti-bonding character, and is stabilized more than the HOMO is destabilized with increasing bondlength. At 1.85 Å the size of the HOMO-LUMO gap is 4.05 eV which implies that the odd electron resides primarily on nickel. In contrast to the HOMO, the LUMO contains significant 4p as well as 4s character in the bonding directions;

B_1 Molecular Orbital:

$$\psi \underset{\underline{\text{HOMO}}}{1.85\ \text{Å}} \text{ doublet} = (0.78)(d_{yz}) + (0.19)(4p_z) + (0.63)(N2p_z)$$

A_1 Molecular Orbital:

$$\psi\ 1.85\ \text{Å doublet} = (0.23)(d_{x^2-y^2}) + (0.13)(d_{z^2}) - (0.69)(4s) - (0.64)(4p_y)$$

$$\underline{\text{LUMO}} \quad -(0.09)(N2s) + (0.35)(N2p_y) - (0.8)(H_{1,2}\,1s)$$

The figure below attempts to illustrate the two possibilities for $Ni-NH_2$ bond formation. In the planer $^2A_1$ molecule there is sigma bonding in y axis, and pi backbonding to nickel from nitrogen in the z axis. In the perpendicular configuration, $^2B_1$, the pi bonding occurs in the NH_2 molecular plane. Coordination of nickel to the B_1 ground state of NH_2 would require an odd electron, or hole in the nickel $4d_{z^2}$ orbital.

Possible $Ni-NH_2$ Configurations

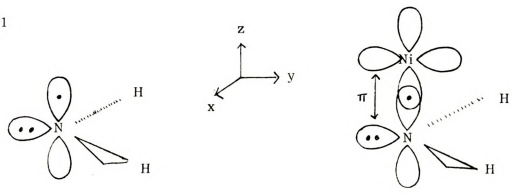

$^1A_1$

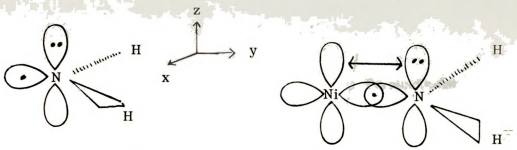

The EHMO calculated lowest energy configuration is planar, or $^1A_1$ (Figure 13). Hybridization and atomic charges of nickel in the two $^2B_1$ and $^1A_1$ configurations, and of nitrogen in the same configurations as well as in bare NH_2 are given below:

Planar $NiNH_2$

Nickel:	$4s^{0.70}$	$4p_x{}^{0.0}$	$4p_y{}^{0.1}$	$4p_z{}^{0.1}$	
	$3d_{xy}{}^{2.0}$	$3d_{xz}{}^{2.0}$	$3d_{yz}{}^{1.4}$	$3d_{x^2-y^2}{}^{1.8}$	$3d_{z^2}{}^{1.9}$
Nitrogen:	$2s^{1.3}$	$2p_x{}^{1.1}$	$2p_y{}^{1.1}$	$2p_z{}^{1.4}$	

Perpendicular $NiNH_2$

Nickel:	$4s^{0.50}$	$4p_x{}^{0.04}$	$4p_y{}^{0.1}$	$4p_z{}^{0.2}$	
	$3d_{xy}{}^{2.0}$	$3d_{xz}{}^{2.0}$	$3d_{yz}{}^{1.8}$	$3d_{x^2-y^2}{}^{2.0}$	$3d_{z^2}{}^{1.3}$
Nitrogen:	$2s^{1.3}$	$2p_x{}^{1.1}$	$2p_y{}^{1.4}$	$2p_z{}^{1.4}$	

Bare NH_2

Nitrogen:	$2s^{1.42}$	$2p_x{}^{1.09}$	$2p_y{}^{1.72}$	$2p_z{}^{1.0}$

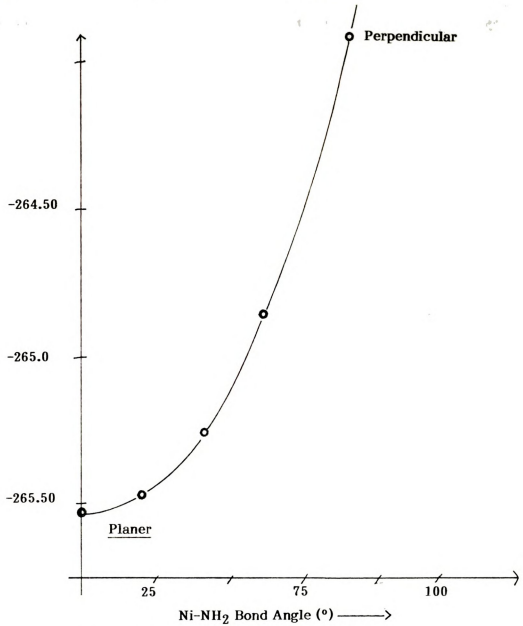

Figure 13. $NiNH_2$, Energy vs. $Ni-NH_2$ Bond Angle

Atom	Atomic Charges (electrons)		
	Planar	Perpendicular	Bare NH_2
Nickel	-0.13	+0.11	-
Nitrogen	-0.22	-0.49	-.40
Hydrogen	+0.18	+0.19	+.20

The extent of positive charge on the hydrogen is nearly equal to that in NH_2 and is about the same for both configurations. The significant change is in the charges on nickel and nitrogen. Nickel changes from negative 0.13 in planar to positive 0.11 in perpendicular. All of this charge has been transferred onto nitrogen. Hybridizations indicate that the extra electron density on nitrogen is all "placed into" the $2p_y$ orbital, which is pi bonding in this coordinate system. Sigma bonding in the perpendicular geometry is through nitrogen 2p unpaired electron and the nickel 4s and $3dz^2$ orbitals.

Since bond formation is between unpaired electrons of nickel and nitrogen, and since the ground state Ni-NH_2 is planar; this bond can be described as occuring between nitrogen and the excited state of NH_2. Stated more explicitly, the EHMO theory predicts this type of bonding. The EHMO theory also places the $4s^13d^9$ electronic configuration much lower than the $4s^23d^8$, whereas experimentally they are degenerate because of correlation effects. This very important class of nickel interactions is being neglected. Thus, the above prediction is correct within the confines of EHMO theory.

The prediction would be more likely to be correct for the Ni^+ ion than the neutral because, in general, there is a greater energy gap between electronic configurations of ions than neutrals.

The fact that pi bonding is more substantial in the unstable configuration indicates that it is not the only determining factor for the geometry.

Ethyl Fragment

The C_2H_5 fragment is constructed with tetrahedral bond angles, and experimentally correct bond lengths. Both carbons acquire a small negative charge.

Nickel Ethyl Fragment

With carbon in tetrahedral coordination, nickel-ethyl bond lengths are 1.90 Å and 2.15 Å for ground state doublet and quartet states respectively, Figure **14**.

The staggered conformation is more stable than the eclipsed by 4.2 kcal/mole. This is about the same as the EHMO theory barrier to rotation for ethane, which is 2-3 kcal/mole.

Next, the nickel-carbon-carbon bond angle was varied from 70° to 130° with all other atoms stationary. Preferred geometry is tetrahedral - 109.470°.

The ethyl fragment changes little upon bonding to nickel. The changes in bonding electron density are small and not significant. Changes in atom charge are also very small.

NH_2-Ni-C_2H_5

The intermediate which is proposed for the metal ion insertion reaction is next assembled from the fragments. Bond lengths and angles determined previously guide the determination of geometry here. These variables, and the axis system are summarized below in Table 13.

The first variable is twist of Ni-NH_2. The local symmetry of N-Ni-C_1-C_2 creates a "molecular plane" since these atoms all lie in the xy plane. With N-Ni-C_1 linear (ψ = 180°), are the NH_2 hydrogens in the xy plane or do they project in the z direction? The most stable EHMO configuration is

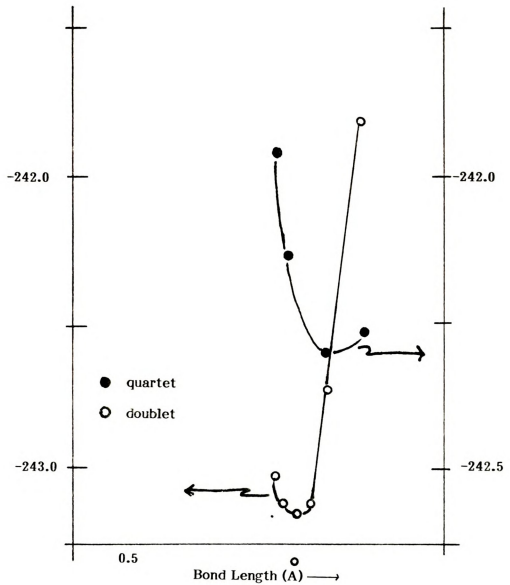

Figure 14. Ni-C_2H_5; Energy vs. Bond Length

Table 13. Geometry Summary of H_2N-Ni-C_2H_5

Angle θ °	Angle ψ °	NH_2 Perpendicular to Z plane?	Energy (EV) $E_{Hückel}$	$E_{repulsion}$	E_{Total}
109.471	180	no	-539.37560	+14.24170	-525.13388
109.471	180	yes	-541.86320	+ 8.92352	-532.93968
90	180	no	-540.98715	8.65496	-532.33219
90*	180	yes	-542.19171	+ 8.72524	-533.46647
90	150	yes	-539.69655	+ 7.24380	-532.52728

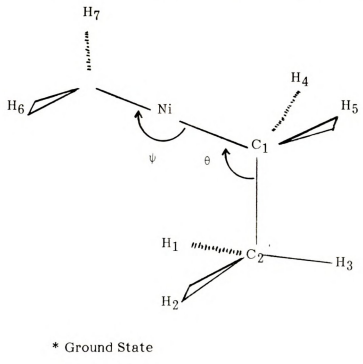

xy plane defined by N, Ni, C_1, C_2, H_3

* Ground State

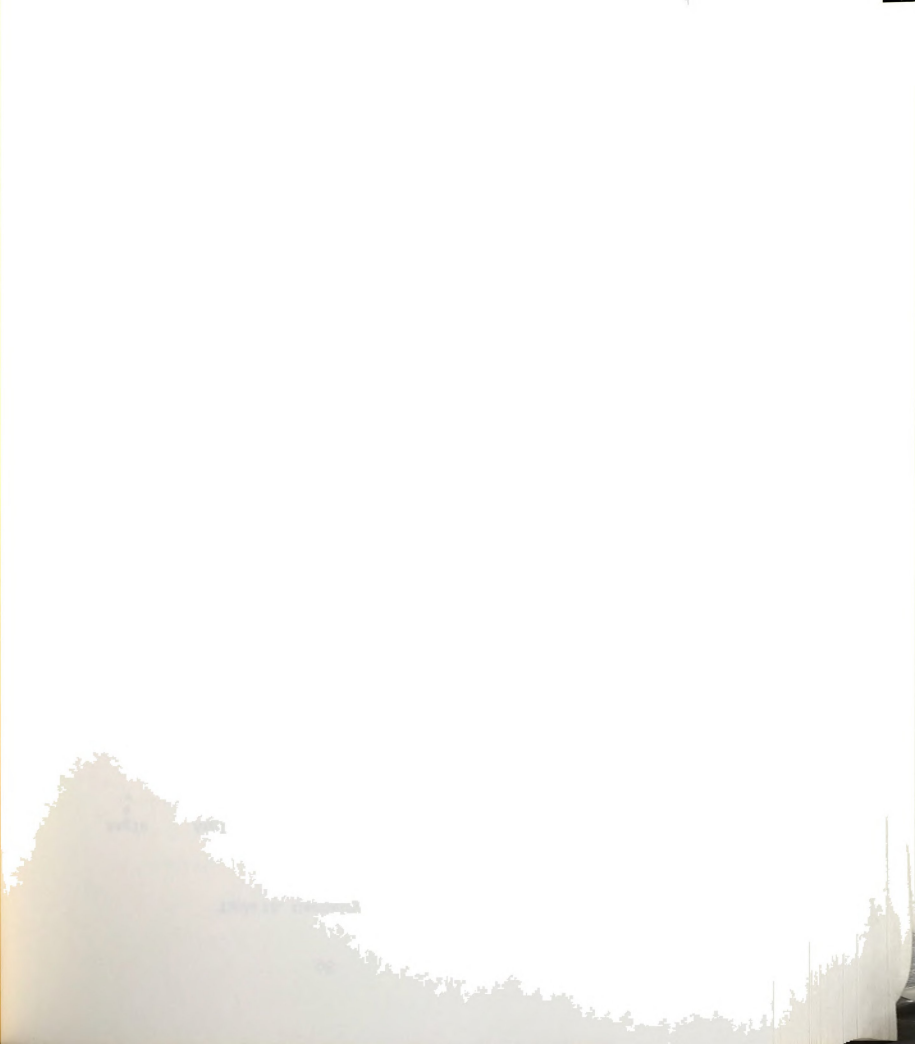

with hydrogens pointing into z plane. Both Hückel and Andersen repulsion terms favor this geometry.

Next the Ni-C_1-C_2 bond is reduced from 109.470 to 90°. This 90° configuration is more stable than with tetrahedral carbon. Again hydrogens project into the z plane.

Finally, with σ = 90°, the N-Ni-C_1 bond is reduced from 180° to 150°. The equilibrium bond angle for the experimentally correct multiplicty of NiH_2 is 150°, and so this angle was also checked. This configuration was not as stable as the previous configuration.

The above described geometries are only a first level of evaluation. They reflect the variables most important in each fragment. Therefore, the lowest energy configuration should reflect important aspects in bonding. Several output parameters are examined to determine their relative importance.

The traditional indication of bond strength is electron density between atoms. These are summarized in Table 14. This analysis indicates that maximizing bond strength/orbital overlap is not a critical variable, since the numbers are nearly the same for all geometries.

Atom charges do provide some guidance. These values change considerably with geometry (Table 15). The lowest energy configuration has nitrogen and nickel charges closest to that in the stable Ni-NH_2 configurations, nitrogen is most negative for least positive nickel. Therefore, this suggests that the intermediate's geometry is influenced by the presence of NH_2 (note that σ = 90° was unstable for Ni-C_2H_5). By analogy to $NiNH_2$ the bond may be considered to be to the NH_2 excited state, as it was in the Ni-NH_2 system. As with nickel amide, the small positive charge on nickel is due to transfer of nitrogen pi electrons. In an indirect way, then,

Table 14. Summary of Electron Density Between Atoms: NH_2-Ni-C_2H_5

Angle θ	Angle ψ	NH_2 Perpendicular	Ni-N	Ni-C_1	Ni-C_2	Ni-$H_{1,2}$	C_2-$H_{1,2}$	N-H	C_1-C_2
NH_2-Ni-C_2H_5:									
*90	180	yes	.33	.25	0.00	0.00	.40	.38	.37
90	180	no	.33	.26	-0.03	0.00	.40	.38	.38
109.47	180	no	.21	.29	0.0	0.0	.40	.38, .29	.38
109.47	180	yes	.33	.29	0.03	0.0	.40	.38	.36
90	150	yes	.36	.28	0.02	0.02	.40	.34	.37
Ni-NH_2:		-	0.34	-	-	-	0.37	-	-
Ni-C_2H_5:		-	-	0.28	0.0	0.0	0.40	-	0.39

*ground state

Table 15. Summary of Atomic Charges: NH_2-Ni-C_2H_5

Angle θ °	Angle ψ °	$NH_2 \perp$	N	Ni	C_1	C_2	Amide H
*90	180	yes	-0.30	+0.10	-0.30	-0.02	+0.17
90	180	no	-0.07	+0.18	-0.51	-0.08	+0.17
109.47	180	no	-0.44	+0.42	-0.50	-0.11	+0.19, +0.26
109.47	180	yes	-0.13	0.17	-0.47	-0.06	+0.17
90	150	yes	-0.25	+0.20	-0.41	-0.05	+0.18

* ground state

pi bonding does influence geometry.

Indications of nickel "hybridization" are given by atomic oribtal in-situ occupancies which are summarized below:

Compound	4s	4p	3d
$Ni\text{-}NH_2$	.69	.25	9.1
$Ni\text{-}C_2H_5$	.62	.07	9.22
$NH_2Ni\text{-}C_2H_5$	.79	.38	8.61

In the original hydride study, "sp hybridization" increased from 0.79 in NiH to 0.95 in NiH_2. D orbital electron density decreased from 9.1 to 8.7. Recall that these numbers for hybridization are actually the number of electrons in each atomic orbital, as indicated by the overlap and electron density matrices. As such, they are not the actual hybridization, but the best approximation offered by EHMO theory. These results mimicked those of ab-inito and MINDO calculations. In the amide study the initial, averaged sp hybridization of 0.81 increases to 1.17 and d electron occupation decreases to 8.6 from about 9.2. It can therefore be concluded that the EHMO theory predicts that the intermediate for metal ion insertion has an sp hybridized, doubly bonded metal center. Figure 15 depicts all the major interactions.

(i) $Ni\text{-}NH_2$ Bond Strength

Comparison of bonding densities (Table 14) of the fragments shows a small reduction in Ni-R bond strength for both bonds in the doubly vs. singly bonded species. This is to be expected since bonding electrons are distributed over more atoms in the intermediate than in the fragments. The reduction is greater for the $Ni\text{-}C_1$ bond than for Ni-N. This could indicate

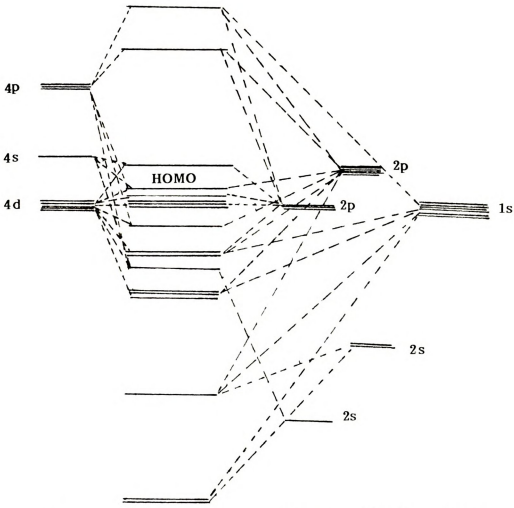

Figure 15. NH_2-Ni-C_2H_5 Molecular Orbital Diagram

that the Ni-NH_2 bond actually is stronger than the Ni-C_2H_5 bond. However, there is considerable risk in making such a conclusion since, at the very least, geometry has not been fully optimized and Ni-C_2H_5 bond density would change with configuration.

These crude estimates of bonding density (by electron distribution between atoms), indicate that the nickel-aminde bond strength is not unusually weak. The value 0.34 is close to that of C_1-C_2 or N-H. If this value is truely representative of bond strength, the estimates of bond strength from ICR experiments conflict. For example, the ICR data base for the Ni^+ ion has 48 ± 5 and < 32 kcal/mole bond strengths for Ni-CH_3 and Ni-NH_2 respectively. This is the opposite ranking of bond strengths which are suggested by EHMO theory. In addition to intrinsic deficiencies in the EHMO theory, one possible explanation for this is that Ni-NH_2 calculations indicate that the bond, apparently, is to an excited state of the amine. The energy to form this bonding state must be accounted for in the closed thermodynamic cycle; and would give an apparent measured weak bond strength:

$$\text{Amide} \longrightarrow \text{Amide}^*$$

State:	nonbonding	bonding
Local symmetry:	$^2B_1$	$^1A_1$

for the process:

$$D^\circ(\text{Ni-NH}_2)_{\text{experimental}} = D^\circ(\text{Ni-NH}_2)_{\text{real}} - \text{Promotion Energy } \Delta E(\text{"}^2B_1\text{"} \longrightarrow \text{"}^1A_1\text{"})$$

Another possibility, of course, pertains to the many excited states of

nickel. Promotion to these electronic configurations would have the same effect of lowering the measured bond energy:

$$D^{o}(Ni\text{-}NH_2) = D^{o}(Ni\text{-}NH_2)_{\text{experimental}} - \text{Promotion Energies}_{\text{real}}$$

$$\Delta E(\text{"}^2B_1\text{"} \longrightarrow \text{"}^1A_1\text{"})$$

or

$$\Delta E(Ni3d^n \longrightarrow Ni4s^1 4p^1 3d^{n-2})$$

Unfortunately, a deficiency of the EHMO theory is that the role of these low lying states of the nickel atom cannot be dealt with.

As a result, it can be said that within the confines of EHMO theory, excited states of both NH_2 and nickel may account for the unusually low experimental values of the $Ni\text{-}NH_2$ bond strength.

(ii) β-Hydrogen Shift

The Table 16 below is a listing of atomic orbital overlaps at the equilibrium geometry. These are a crude estimate of nonbonded interactions, but they have some interesting features. A somewhat surprising feature is the significant nickel interactions with carbon 2 and hydrogens 1,2 primarily in the xy plane. One might anticipate a large overlap with neighboring orbitals since nickel 4s and 4p orbitals are very spatially extended. For the proposed metal-ion insertion intermediate, the overlap is not significant since the orbitals haven't any electrons in them. However, such interactions would become important for the second step of the proposed metal insertion reaction - β hydrogen shift at which point electrons would move into these orbitals. For the hydrogens, the overlap is greatest in the y direction which is the direction of hydrogen transfer from carbon to nickel. Apparently, the geometry of the intermediate is appropriate for the next step of atom transfer. Note also that with amide nitrogens above and below the xy plane

Table 16. Overlap in Atomic Orbitals for NH_2–Ni–C_2H_7, Equilibrium Geometry

Atom	Nickel Orbital								
	4s	4px	4py	4pz	$3dx^2-y^2$	$3dz^2$	3dxy	3dxz	3dyz
Nitrogen									
2s	.282	.483	-	-					
2px	.217	-	-	-					
2py	-	-	.166	-					
2pz	-	-	-	.167					
Carbon 1									
2s	.329	.546	.225	-					
2px	.284	.115	-	-					
2py	-	-	-	-					
2pz	-	-	-	.225					
Carbon 2						0			
2s	-	.341	.277	-					
2px	.138	-	.165	-					
2py	.111	.165	-	-					
2pz	-	-	-	.137					
H_3	-	-	-	-					
H_1	.115	.191	.264	.124					
H_2	.115	.191	.264	.124					
H_5	.101	.306	-	.114					
H_4	.101	.306	-	.114					
H_6	.101	.313	-	.101					
H_7	.101	.313	-	.101					

the hydrogen can shift onto nickel into this plane with a minimum of repulsive interactions.

SUMMARY

SUMMARY

In the past several years an extensive body of literature has appeared in the area of gas phase organometallic ion/molecule reactions. Most of the observed reactions can be explained by assuming that the first step of the interaction is metal ion insertion into a bond of an organic molecule.

Ion Cyclotron Resonance Spectrometry investigations of reactions of first row transition metal ions with the primary amine, n-propyl amine, parallel the literature in that for other types of organic molecules, selectivity in the insertion step is characteristic of the particular metal ion. An explanation of the reactivity trends of the 1st row transition metal ions is suggested based on the thermodynamics of the metal insertion process and on the electronic configurations of the metal which are conducive to formation of the reaction intermediate.

If it is assumed that 2 electrons outside the metal's 3d shell are required for formation of the intermediate, suitable low lying electronic configurations would be the $4s^2 3d^n$ and the $4s^1 4p^1 3d^n$. A ranking of the first row metal ions based on the promotion energy to achieve these configurations matches, inversely, the ordering of the relative reactivities in gas phase ion/molecule reactions:

$$Fe^+, Co^+, Cr^+ \sim Ni^+, \quad Mn^+, Zn^+, Cu^+$$

Increasing Promotion Energy ⟶

⟵ **Increasing Reactivity**

This ordering suggests that ions with higher promotion energies are less reactive, or more selective of the bonds into which insertion occurs because the energetics of formation of the intermediate are affected by the energy to rearrange electrons:

Total Reaction Enthalpy = Energy In - Energy Back - Rearrangement Energy

This assumes that once in the appropriate M^{+*} configuration, all M^{+*}-R bonds have the same strength for a given R.

Extended Hückel molecular orbital theory was used to examine the bonding of the intermediate, using zero valent nickel as the metal center. It was found that bonding occurs primarily through nickel 4s and 4p orbitals. This is attributed to the greater radial extension and therefore greater orbital overlap of the 4s and 4p in comparison to the 3d.

REFERENCES

LIST OF REFERENCES

1. J.L. Beauchamp, Ann. Rev. Phys. Chem., 22, 527 (1971).
2. J.D. Baldeschweiler, Science, 159, 263 (1968).
3. J.D. Baldeschweiler, S.S. Woodgate, Acc. Chem. Res., 4, 114 (1971).
4. C.J. Drewery, G.C. Goode, K.R. Jennings, "Ion Cyclotron Mass Spectrometry", MTP International Review of Science - Physical Chemistry, Series One, Volume 5, Mass Spectrometry, A. Macoll, Ed., University Park Press, Baltimore, 183 (1972).
5. T.A. Lehman, M.M. Bursey, Ion Cyclotron Resonance Spectroscopy, J.Wiley and Sons, New York (1976).
6. J.M.S. Henis, "Ion Cyclotron Resonance Spectrometry", Ion-Molecule Reactions, Vol. 2, J.L. Franklin, Ed., Plenum Press, New York, 395 (1972).
7. G.C. Goode, A.J. Ferrer-Correia, K.R. Jennings, Int. J. Mass. Spec. Ion Phys., 5, 229 (1970).
8. J. Allison, Ph.D. Thesis, 1976.
9. H.J. Svec, G.A. Junk, Z. Naturforsch, 23 1 (1968).
10. R.E. Winter, R.W. Kiser, J. Inorg. Chem., 3 699 (1964).
11. E. Schumacher, R. Taubenest, Helv. Chim. Acta, 47, 1525 (1964).
12. M.S. Foster, J.L. Beauchamp, J. Am. Chem. Soc., 93, 4924 (1971).
13. J. Muller, "Ion Molecule Reactions of Organometallic Complexes", Advances in Mass Spectrometry, Vol. 6, A.R. West, Ed., Appl. Sci. Publishers, Ltd., England, 823 (1974).

LIST OF REFERENCES

1. J.L. Beauchamp, Ann. Rev. Phys. Chem., 22, 527 (1971).
2. J.D. Baldeschweiler, Science, 159, 263 (1968).
3. J.D. Baldeschweiler, S.S. Woodgate, Acc. Chem. Res., 4, 114 (1971).
4. C.J. Drewery, G.C. Goode, K.R. Jennings, "Ion Cyclotron Mass Spectrometry", MTP International Review of Science - Physical Chemistry, Series One, Volume 5, Mass Spectrometry, A. Macoll, Ed., University Park Press, Baltimore, 183 (1972).
5. T.A. Lehman, M.M. Bursey, Ion Cyclotron Resonance Spectroscopy, J.Wiley and Sons, New York (1976).
6. J.M.S. Henis, "Ion Cyclotron Resonance Spectrometry", Ion-Molecule Reactions, Vol. 2, J.L. Franklin, Ed., Plenum Press, New York, 395 (1972).
7. G.C. Goode, A.J. Ferrer-Correia, K.R. Jennings, Int. J. Mass. Spec. Ion Phys., 5, 229 (1970).
8. J. Allison, Ph.D. Thesis, 1976.
9. H.J. Svec, G.A. Junk, Z. Naturforsch, 23 1 (1968).
10. R.E. Winter, R.W. Kiser, J. Inorg. Chem., 3 699 (1964).
11. E. Schumacher, R. Taubenest, Helv. Chim. Acta, 47, 1525 (1964).
12. M.S. Foster, J.L. Beauchamp, J. Am. Chem. Soc., 93, 4924 (1971).
13. J. Muller, "Ion Molecule Reactions of Organometallic Complexes", Advances in Mass Spectrometry, Vol. 6, A.R. West, Ed., Appl. Sci. Publishers, Ltd., England, 823 (1974).

14. J. Allison, D.P. Ridge, J. Organometal. Chem., 99, C-11 (1975).

15. J. Allison, D.P. Ridge, J. Am. chem. Soc., 99, 35 (1977).

16. H. Hartmann, K.P. Wanczek, Ion Cyclotron Resonance Spectrometry II; Lecture Notes in Chemistry, G. Berthier, Eds., Spingler-Verlag, Berlin Heidelberg Pub., 108 (1982).

17. L.F. Halle, P.B. Armentrout, J.L. Beauchamp, J. Am. Chem. Soc., 103, 963 (1981).

18. R.B. Freas, D.P. Ridge, J. Am. Chem. Soc., 102, 7129 (1980).

19. A.E. Stevens, J.L. Beauchamp, J. Am. Chem. Soc., 101, 6449 (1979).

20. J.W. Warren, Nature, 165 810 (1950).

21. R.E. Winters, R.W. Kiser, Inorg. Chem., 4, 157 (1965).

22. K. Ervin, S.K. Loh, N. Ariston, P.B. Armentrout, J. Am. Chem. Soc., 105, 493, (1983).

23. H. Harmann, op.cit., 145.

24. R.C. Burnier, G.D. Byrd, B.S. Freiser, Anal. Chem., 52 1641 (1980).

25. R.W. Jones, R.H. Staley, J. Am. Chem. Soc., 102, 3794 (1980).

26. A.E. Stevens, J.L. Beauchamp, J. Am. Chem. Soc., 103, 190 (1981).

27. T.J. Carlin, L. Sallans, C.J. Cassady, D.B. Jacobson, B.S. Freiser, J. Am. Chem. Soc., 105, 6320 (1983).

28. D.B. Jacobson, B.S. Freiser, J. Am. Chem. Soc., 105, 5197 (1983).

29. D.B. Jacobson, B.S. Freiser, J. Am. Chem. Soc., 105, 7492 (1983).

30. J. Allison, D.P. Ridge, J. Am. Chem. Soc., 101, 4998 (1979).

31. P.B. Armentrout, J.L. Beauchamp, J. Am. Chem. Soc., 103, 784 (1981).

32. P.B. Armentrout, L.F. Halle, J.L. Beauchamp, J. Am. Chem. Soc., 103, 6624 (1981).

33. P.B. Armentrout, J.L. Beauchamp, J. Am. Chem. Soc., 103 6628 (1981).

34. G.H. Weddle, J. Allison, D.P. Ridge, J. Am. Chem. Soc., 99, 105 (1977).

35. P.B. Armentrout, J.L. Beauchamp, J. Am. Chem. Soc., 102, 1736 (1980).

36. M.S. Foster, J.L. Beauchamp, J. Am. Chem. Soc., 93, 4924 (1971).

37. M.S. Foster, J.L. Beauchamp, J. Amc. Chem. Soc., 97, 4808 (1975).

38. D.B. Jacobsen, B.S. Freiser, J. Am. Chem. Soc., 105 7484 (1983).

39. M.S. Foster, J.L. Beauchamp, J. Am. Chem. Soc., 97, 4814 (1975).

40. T.J. Jackson, D.B. Jacobsen, B.S. Freiser, J. Am. Chem. Soc., 106, 1252 (1984).

41. L.F. Halle, R. Houriet, M. Kappes, R. Staley, J.L. Beauchamp, J. Am. Chem. Soc., 104, 6293 (1982).

42. D.B. Jacobsen, B.S. Freiser, J. Am. Chem. Soc., 105, 736 (1983).

43. P.L. Po, T.P. Radus, R.F. Porter, J. Phys. Chem., 82, 5, 520 (1978).

44. J.K. Burdett, Molecular Shapes, Theoretical Models of Inorganic Stereochemistry, Wiley-Interscience Publication, John-Wiley and Sons, New York, 1980, p. 158.

45. J.E. Huheey, Inorganic Chemistry, Principles of Structure and Reactivity, Harper and Row Publishers, New York, NY, p. 573 (1978).

46. K.F. Purcell, J.C. Kotz, Inorganic Chemistry, W.B. Saunders Publishing Company, Philadelphia, PA, p. 120 (1977).

47. P.B. Armentrout, L.F. Halle, J.L. Beauchamp, J. Am. Chem. Soc., 103, 6501 (1981).

48. W.L. Grady, M.M. Bursey, Int. J. Mass. Spec. Ion Proc., 55, 111 (1983/84).

49. W.L. Grady, M.M. Bursey, Int. J. Mass Spec. Ion Proc., 56, 161 (1984).

50. W.L. Grady, M.M. Bursey, Int. J. Mass Spec. Ion Proc., 52, 247 (1983).

51. W.L. Brody, M.M. Bursey, Int. J. Mass Spec. Ion Proc., 52, 259 (1983).

52. E.S. Ackerman, W.L. Grady, M.M. Bursey, Int. J. Mass Spec Ion Proc., 55, 275 (1983).

53. B. Radecki, J. Allison, J. Am. Chem. Soc., 106, 946 (1984).

54. R.C. Burnier, T.J. Carlin, W.D. Reents, R.B. Cody, R.K. Lengel, B.S. Freiser, J. Am. Chem. Soc., 101, 7127 (1979).

55. P.M. Holland, A.W. Castleman, J. Am. Chem. Soc., 102, 6174 (1980); P.M. Holland, A.W. Castlemann, D.M. Lindsey, K.I. Peterson, J. Am. Chem. Soc., 100, 6039 (1978).

56. L.M. Bass, D. Cates, M.F. Jarrold, N.J. Kirchner, M.T. Bowers, J. Am. Chem. Soc., 105, 7024 (1983).

57. C.E. Moore, Atomic Energy Levels, Vol. II, Circ. Nat. Bur. Stand., 467, U.S. Government Printing Office, Washington, DC (1952).

58. L.E. Orgel, J. Chem. Soc., 4186, (1958).

59. D.M.P. Mingos, J.C.S., Chem. Comm., p. 165 (1972).

60. J. Chatt, B.L. Shaw, J. Chem. Soc., 705 (1959).

61. N. Rosch, R. Hoffman, Inorg. Chem., 13, 11, 2656 (1974).

62. T.A. Albright, R. Hoffmann, J.C. Thibeault, D.L. Thorn, J. Am. Chem. Soc., 101, 3801 (1979).

63. O. Eisenstein, R. Hoffman, J. Am. Chem. Soc., 103, 5582 (1981).

64. R. Hoffman, M. Chen, M. Elian, A. Rossi, D. Mingos, Inorg. Chem., 13, 2666 (1974).

65. R. Summerville, R. Hoffmann, J. Am. Chem. Soc., 101, 3821 (1979).

66. T. Albright, R. Hoffmann, J. Am. Chem. Soc., 100, 7736 (1978).

67. T. Albright, R. Hoffmann, Y. Tse, T. D'Offavio, J. Am. Chem. Soc., 101, 3812 (1979).

68. O. Eisenstein, R. Hoffmann, 102, 6148 (1980).

69. R. Hoffmann, Ang. Chem., 21, 10, 711 (1982).

70. A. Anderson, J. Chem. Phys., 65, 5, 1729 (1976).

71. A. Anderson, J. Am. Chem. Soc., 100, 1153 (1978).

72. T. Wittrig, P.D. Szuromi, W.H. Weinberg, J. Chem. Phys., 76, 6, 3306

(1982).

73. W.J. Moore, "Physical Chemistry", Prentice Hall Inc. Publishers, London, p. 614-745, (1972).

74. J.K. Burdett, op. cit., p. 2-20.

75. R. Hoffman, J. Chem. Phys., 39, 6, 1397 (1963).

76. A.B. Andersen, J. Chem. Phys., 62, 3, 1187 (1975).

77. A.B. Andersen, J. Chem. Phys., 68, 4, 1744 (1978).

78. B. Rosen, Ed., Selected Constants, Spectroscopic Data Relative to Diatomic Molecules, Permagon, New York, (1970).

79. K.P. Huber, G. Herzberg, Molecular Spectra and Molecular Structure, Vol. 4, Van Nostrand-Reinhold, New York, (1979).

80. F. Ruette, G. Blyholder, J. Head, J. Chem. Phys., 80, 5, 3042 (1984).

81. J. Demuynek, H.F. Schaefer III, J. Chem. Phys., 72, 1, 311 (1980).

82. J. Tyrrell, A. Youakim, J. Phys. Chem., 84, 3568 (1980).

83. J. Tyrell, A. Youakim, J. Phys. Chem., 85, 3614 (1981).

84. M. Blomberg, P.E.M. Siegbahn, J. Chem. Phys., 78, 986 (1983).

85. M. Blomberg, P.E.M. Siegbahn, B.O. Roos, Mol. Phys., 47, 127 (1982).

86. M.B. Hall, Inorg. Chem., 17, 8, 2261 (1978).

87. M.B. Hall, Inorg. Chem., 17, 8, 2371 (1978).

88. Tables of Interatomic Distances and Configurations in Molecules and Ions, Special Publication #11, 1958.

89. M.F. Lappert, P.P. Power, A.R. Sanger, R.C. Srivastava, Metal and Metalloid Amides, John Wiley & Sons, Publisher, New York, 1980.

90. S.K. Huang, J. Allison, Organometalics, 2, 883 (1983).

91. R.C. Burnier, T.J. Carlin, W.D. Reents, R.B. Cody, R.K. Lengel, B.S. Freiser, J. Am. Chem. Soc., 101, 7027, (1979).

92. C.J. Cassady, B.S. Freiser, S.W. McElvany, J. Allison, submitted to J. Am. Chem. Soc.

93. J.S. Uppal, R.H. Staley, J. Am. Chem. Soc., 104, 1238 (1982).